Limina — The Journal of UAP Studies

http://limina.uapstudies.org/ | https://limina.scholasticahq.com/

Magnetoplasmadynamic Unidentified Aerial Phenomena: Basic Physics, Diagnostics and Research Methodology

Massimo Teodorani, Ph.D.*

Society for UAP Studies

https://orcid.org/0009-0000-7706-7455

ARTICLE INFO

Received: 03 September 2025
Received in revised form: 10 December 2025
Accepted: 27 February 2026

**Author contact: mlteodorani@alice.it*

ABSTRACT

This paper—best classified as a review and methodological framework rather than a traditional research article—presents a physics-based observational platform for coordinated, multi-modal study of transient aerial phenomena. Rather than reporting new observations, it synthesizes plasma, radiative, and magnetohydrodynamic diagnostics into a unified experimental strategy. Building on prior theoretical analyses, it develops a comprehensive model incorporating high-field magnetohydrodynamics, plasma confinement, radar interaction, spectroscopic signatures, and electromagnetic effects. Central to this framework is the working hypothesis that the phenomenon is enveloped by a variably modulated magnetic field (10–1000 T) capable of stabilizing a plasma sheath, shaping radiative output, and influencing the surrounding atmosphere. With particular emphasis on optical/IR photometry and spectroscopy, the paper formulates testable hypotheses and outlines the corresponding measurement protocols. These include Zeeman spectroscopy for magnetic-field diagnostics, microwave reflectivity for assessing radar cross-section variability, and coordinated electromagnetic and biophysical monitoring to evaluate potential exposure effects. Potential ground interactions—localized thermal, magnetic, or chemical changes—are noted as supplemental diagnostic avenues. By combining physical modeling with a structured observational methodology, this work provides a coherent, physics-grounded roadmap for identifying, monitoring, and characterizing UAP events, and for distinguishing conventional atmospheric or technological sources from anomalous, field-modulated phenomena.

1. Introduction

The phenomenon under investigation can be most effectively approached using the framework of plasma astrophysics and high-energy laboratory plasma research (NASEM 2007). If UAP manifestations are indeed governed by magnetoplasmadynamic processes, their observational characteristics—luminosity, spectral variability, radar cross-section, and anomalous flight dynamics—can be modeled as emergent effects of strongly coupled magnetohydrodynamic (MHD) systems interacting with the atmosphere. The study of such systems requires precise formulation of boundary conditions (object surface vs. plasma sheath), field strengths, and plasma parameters such as density, temperature, collision frequency, and optical depth. By establishing a controlled diagnostic methodology—spanning ground-based spectrometry, high-speed imaging, multi-band radar interrogation, and magnetometric sensing—it becomes possible to distinguish between conventional atmospheric plasma phenomena and anomalous sources consistent with artificial field modulation.

The phenomenon of unidentified flying objects, more recently termed Unidentified Aerial Phenomena (UAP), continues to generate significant scientific (Coumbe 2023; Haines, 2000; Knuth *et al.* 2025; NASA 2023; NICAP 1964; ODNI 2021; Strand 1984; Teodorani 2024; Watters *et al.* 2023) and public interest. Numerous declassified reports, pilot testimonies, radar data, and sensor logs document encounters with airborne objects exhibiting extraordinary maneuverability, luminous intensity, and electromagnetic properties inconsistent with known aerospace technologies (Project Condign 2000). The aim of this paper is to unify fragmented empirical and anecdotal evidence into a coherent scientific framework grounded in physical principles.

We adopt as a recurring physical model a compact, disc-shaped craft with a diameter of approximately 5–10 meters, enveloped in a magnetically confined plasma sheath sustained by dynamic magnetic fields with strengths ranging from 10 to 1000 tesla (Neukart 2023; Peratt 1992). The underlying assumption is that the core structure is composed of advanced superconducting metamaterials, capable of maintaining extreme current densities with negligible resistive losses (Choueiri 2009). These materials would generate intense toroidal magnetic fields, confining an ionized plasma envelope that in turn stabilizes itself through interaction with a strong electric field flowing across the craft's surface (Bellan 2006; Chen 2016). Such a system would provide multiple functional advantages, including aerodynamic shielding, stealth through radar absorption (Zhang 2021), electromagnetic emission control, and potential propulsion through magnetohydrodynamic (MHD) mechanisms (Maccabee, 1994; Meessen 2012a; 2012b; NASA NTRS; Tajmar 2002; Tkachenko *et al.* 2023).

From a spectroscopic standpoint, the plasma envelope offers a direct opportunity for measurement. A primary diagnostic tool is the Zeeman effect, in which the strong magnetic field induces spectral line splitting (Zeeman 1897; Jefferies and Mickey 1991; Lang 1991). By measuring the separation of characteristic emission lines in the visible, infrared, or ultraviolet range, one could directly estimate the field strength surrounding the object. For a magnetic field on the order of 100 T, line separations on the scale of 10^{-2} Å become resolvable with high-dispersion spectrographs (Landi Degl'Innocenti and Landolfi 2004), providing a plausible observational pathway to confirm the presence of such extreme fields.

Reports of UAPs frequently describe silent operation, abrupt accelerations, sharp turns, and hovering in the absence of aerodynamic support (Hendry 1979; Knuth *et al.* 2019; ODNI 2021). Conventional propulsion systems cannot fully explain these behaviors. One physically consistent approach considers the coupling of strong magnetic fields and plasma sheaths to reduce drag, manipulate ionization in the surrounding air, and vector thrust by controlled Lorentz-force interactions (Goksel and Mashek 2016; Baines *et al.* 2021). The principle is that the flying object produces an intense alternating magnetic field with a supraconductive outer shell. They then ionize air around the UAP in specific locations when the intensity of the magnetic field grows or shrinks. This produces a Lorentz force applied on electrons and ionized air in a huge volume. By the principle of reaction, this applies a force on the flying object (Meessen 2012a, 2012b).

Magnetoplasmadynamic (MPD) thrusters, already tested in laboratory conditions, provide a conceptual parallel: plasma streams are accelerated and expelled by electromagnetic fields, producing directed thrust. By adjusting field geometry, a UAP could theoretically achieve omnidirectional thrust vectoring and rapid maneuverability without aerodynamic control surfaces (NASA NTRS; Tkachenko *et al.* 2023).

The plasma envelope also yields secondary effects consistent with observational reports. As ionized gases interact with ambient air, they generate luminous coronas visible in low-light conditions, radio frequency emissions detectable as broadband bursts, and localized heating sufficient to distort infrared detection (Peratt 1992; Baines *et al.* 2021). The ionized layer acts as both a dielectric medium and a conductive shell, thereby scattering or absorbing incoming electromagnetic radiation (Ginzburg and Rukhadze 1972). This produces stealth-like characteristics in radar observations, including absorption, anomalous scattering, and phase cancellation. Simultaneously, the plasma sheath can serve as a physical barrier: small projectiles or explosive fragments entering the field experience collisional drag, thermal dissipation, and deflection by Lorentz forces, reducing their effective penetration (Cooper 1996; Walters & Zukas 1989).

The theoretical requirements for such a system are extreme but not incompatible with advanced physics. Magnetic confinement of plasma at temperatures exceeding 10^7 K has been demonstrated in controlled fusion experiments, with field strengths of 5–20 T achieved in modern tokamaks and stellarators (Chen 2016; Bellan 2006). Extrapolating to hundreds of Tesla requires either exotic superconductors, compact fusion-based energy generation, or speculative high-density energy storage systems such as superconducting magnetic energy storage (SMES) or advanced thorium reactors (Herlach and Miura 2003; Choueiri 2009). The estimated power budget for a sustained 10 T field combined with plasma heating falls within tens to hundreds of megawatts, suggesting that compact but powerful reactors would be required for continuous operation (Bellan 2006).

Environmental effects provide additional testable predictions. The presence of intense time-varying magnetic fields would induce strong electric fields, disrupting radio communications, GPS navigation, and compass stability (Glover *et al.* 2007; ICNIRP 2020). Observers would detect corona discharges, electromagnetic pulses, and broadband noise. Localized ionization would also produce hazardous radiation and thermal signatures. These phenomena align with documented cases of avionics interference and sensor anomalies reported during UAP encounters (ODNI 2021; Rodeghier 1981).

While speculative, the proposed model is grounded in established principles of plasma physics, magnetohydrodynamics, and superconductivity (Chen 2016; Bellan 2006; Peratt 1992). Parallels exist in terrestrial technologies: NASA's MPD thruster programs (NASA NTRS), plasma stealth experiments conducted in both China and Russia, and plasma confinement techniques in nuclear fusion research (Bellan 2006). Although the hypothesized UAP systems extend far beyond current engineering limits, the convergence of superconducting materials, extreme magnetic confinement, and plasma-based shielding offers a plausible explanatory framework. The resulting craft would possess capabilities consistent with observed UAP behavior, including high maneuverability, stealth (in radar waves, not in the optical range), electromagnetic disruption, and resilience to explosive impacts. Further research into high-intensity magnetic fields, plasma-material interactions, and compact energy systems is essential for advancing our understanding of whether such phenomena can be physically realized.

2. Pure Plasma vs. Solid Object with Plasma Sheath

The observation of luminous phenomena in the atmosphere and outer space raises the fundamental question of whether such manifestations originate from self-organized plasma structures (Fedosin and Kim 2001; Stenhoff 1999) or from solid objects enveloped by plasma and intense magnetic fields (Peratt 1992; Teodorani 2004). Distinguishing between these possibilities is essential, as the underlying nature of the phenomenon has profound implications for energy generation, dynamics, and environmental interactions (Fig. 1). This study addresses the problem through theoretical modeling and observational diagnostics, employing spectroscopy, magnetometry, radar analysis, and thermal imaging (Chen 2016; Bellan 2006). The analysis draws comparisons with natural plasma formations such as atmospheric plasmoids and ball lightning (Peratt 1992; Teodorani, 2004), while considering the possibility of solid UAP-like objects surrounded by magnetoplasma envelopes. The possible confirmation that a UAP is a solid, structured object, identifiable as a flying machine, does not necessarily imply that it represents extraterrestrial technology, although this possibility cannot be ruled out.

The spectral behavior of luminous sources provides the first criterion of distinction. Pure plasma emission (optically thin, spontaneous emission) arises from atomic and ionic transitions in form of emission lines, described as:

$$I(\nu) = \sum_{i,j} h\nu_{ij}\, A_{ij}\, n_i\, \phi_{ij}(\nu)$$

where:

- i, j label atomic energy levels (upper level i, lower level j);
- h is Planck's constant; ν_{ij} is the transition frequency between levels i and j;
- A_{ij} is the Einstein A coefficient for spontaneous emission $i \longrightarrow j$ (units s^{-1});
- n_i is the population density (m^{-3}) of the upper level i;
- $\Phi_{ij}(\nu)$ is the normalized line profile function (Hz^{-1}), *e.g.*, Doppler or Voigt profile, satisfying $\int \Phi_{ij}(\nu) d\nu = 1$.

Whereas a solid body follows Planck's law of blackbody radiation, and represents a thermal continuum given by:

$$B_\lambda(T) = \frac{2hc^2}{\lambda^5} \frac{1}{e^{hc/(\lambda k_B T)} - 1}$$

where:

- $B(\lambda, T)$ is the spectral radiance per unit wavelength of the blackbody (W m^{-2} sr^{-1} m^{-1});
- k_B is the Boltzmann constant;
- T is the absolute temperature in K;
- h: Planck constant;
- c: speed of light in vacuum;
- λ: wavelength.

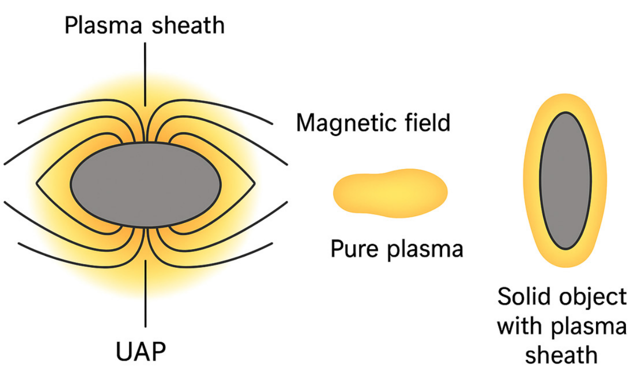

Figure 1. *Sketch of a structured UAP surrounded by a plasma sheath confined by a strong magnetic field.*

A thermal continuum from an opaque surface observed through an overlying, cooler, optically thin plasma will generally show absorption features at the resonant frequencies of the plasma constituents (analogous to Fraunhofer lines in the solar spectrum), because the overlaying gas preferentially absorbs continuum photons at line frequencies. Conversely, emission lines appear when the emitting plasma is seen against a darker background (*e.g.*, off the limb of the solid object) or when the plasma itself is sufficiently hot and optically thick to radiate in excess of the background continuum. Therefore the presence of emission or absorption lines, and their relative strengths, depends strongly on geometry, optical depth, and the temperature/density stratification of the sheath; line profiles must be interpreted using radiative transfer models (absorption coefficient, source function) rather than by a single heuristic statement.

The simultaneous presence of a continuous thermal spectrum overlaid with spectral lines suggests a solid object embedded within a plasma sheath, while the exclusive presence of line spectra indicates pure plasma without a solid substrate (Bellan 2006; Ginzburg and Rukhadze 1972).

Magnetic field diagnostics further refine the classification. Plasma may exist without an external magnetic field, but stable, structured plasma confinement generally implies the action of a coherent and intense magnetic field. Such fields are governed by the Lorentz force:

$$\mathbf{F} = q(\mathbf{E} + \mathbf{v} \times \mathbf{B})$$

where: **F**: Lorentz force acting on the particle; q: electric charge of the particle; **E**: electric field vector; **v**: velocity vector of the particle; **B**: magnetic flux density (magnetic field) vector.

In equilibrium these fields satisfy the magnetohydrodynamic balance:

$$\nabla p = \mathbf{J} \times \mathbf{B}$$

where p is plasma pressure, **J** the current density, and **B** the magnetic field. For fields in the range of 10–1000 T, the associated magnetic pressure:

$$P_B = \frac{B^2}{2\mu_0}$$

where: B is the magnetic flux density; μ_0: permeability of free space,

can exceed 10^8 Pa, sufficient to confine low-density plasma in a toroidal or spherical sheath (Bellan 2006; Chen 2016). Polarimetric and interferometric measurements could detect such coherent fields, with stable, structured magnetism strongly suggesting the presence of a central solid or technological source, in contrast to chaotic, transient fields expected from natural plasmas (Landi Degl'Innocenti and Landolfi 2004; Peratt 1992).

Radar interactions provide another diagnostic. The reflectivity of plasma depends on the electron density through the plasma frequency:

$$\omega_p = \sqrt{\frac{n_e e^2}{\epsilon_0 m_e}}$$

where: ω_p: electron plasma frequency; n_e: electron number density; e: elementary charge; ε_0: vacuum permittivity; m_e: electron rest mass,

with a cutoff condition such that if $\omega < \omega_p$, incident waves are reflected. For a 10 GHz radar ($\omega \approx 6.28\times10^{10}$ rad/s), the critical density is $n_e \approx 1.2\times10^{18}\ \mathrm{m}^{-3}$ (Ginzburg and Rukhadze 1972). A plasma sheath above this density behaves as an opaque barrier, producing radar invisibility or anomalous scattering. Nonlinear refractive indices and density fluctuations further generate incoherent radar returns, ghost targets, or sudden signal disappearance, all of which have been documented in UAP encounters (ODNI 2021). By contrast, solid objects produce radar reflections described by Mie scattering theory, with cross-sections dependent on size relative to wavelength. The presence of sharp, coherent radar reflections is therefore a strong indicator of a solid structure.

Thermal imaging also distinguishes the two categories. A pure plasma cloud exhibits diffuse, incoherent infrared signatures that fluctuate with time and space, whereas a solid object produces a compact and temporally stable thermal emission consistent with localized heat radiation (Peratt 1992; Chen 2016). Similarly, Doppler velocimetry and multi-sensor tracking reveal contrasting kinematic behaviors: natural plasma (Teodorani 2004) displays pulsations, erratic motion, and morphological changes due to instabilities such as Rayleigh–Taylor and Kelvin–Helmholtz modes, while solid objects typically follow coherent, ballistic, or directed trajectories indicative of active propulsion and possible intelligent control (Bellan 2006; Tkachenko *et al.* 2023).

The combined diagnostic approach thus provides robust criteria: plasma-only phenomena manifest discrete emission lines without a continuous spectrum, chaotic or absent magnetic fields, incoherent radar returns, unstable kinematics, and diffuse thermal signatures. Conversely, solid objects enveloped by plasma display a thermal continuum underlying emission lines, coherent and structured magnetic fields, sharp radar reflections when plasma density permits, stable and directed motion, and compact infrared emissions (Peratt 1992). The presence of a strong, coherent magnetic field and a continuous spectral background constitutes the most indicative signature of a plasma-confined solid object (Bellan 2006; Jefferies and Mickey 1991).

3. Luminosity of a Solid Object with Plasma Sheath

The luminosity and spectral appearance of a solid object enveloped by a plasma sheath depend critically on plasma temperature, density, optical depth, and magnetic field configuration. Although strong magnetic fields can influence charge confinement and particle acceleration, the magnitude of the resulting radiation is highly sensitive to these parameters and generally cannot be assumed to be extreme in the absence of direct measurements (Bellan 2006; Chen 2016). Both thermal and non-thermal radiative mechanisms may contribute, but their relative importance remains uncertain.

A first approximation to the thermal component can be obtained from the Stefan–Boltzmann law:

$$L = A\,\sigma\,T^4$$

where A is the effective emitting surface, T is the radiative temperature of the plasma or of the underlying object if the plasma is optically thin and σ is the Stefan-Boltzmann constant.

If the plasma is optically thick (opaque), it absorbs and re-emits the radiation from the inner object, so that the observed luminosity is approximately that of the plasma. If the plasma is optically thin (transparent), the luminosities of the object and the plasma simply add. So the formula above becomes:

$$L_{\text{tot}} = L_{\text{obj}} + L_{\text{plasma}} = \sigma A_{\text{obj}} T_{\text{obj}}^4 + \sigma A_{\text{plasma}} T_{\text{plasma}}^4$$

Considering, for example, a disc-shaped object surrounded by a plasma sheath of approximately 0.5 meters in thickness and embedded in a magnetic field of 100 T, calculations indicate that the intrinsic radiant output results from the combined contributions of thermal Bremsstrahlung and synchrotron emission (Bekefi and Barrett 1977; Peratt 1992).

For moderate temperatures of a few thousand kelvin, radiative luminosities of ~ 1-10 MW are plausible for meter-scale surfaces. These values may increase for larger emitting areas or higher temperatures, but they may also be significantly reduced if the plasma has low optical depth or low particle density.

Non-thermal processes, such as synchrotron emission, require the presence of relativistic electrons. Because no such particle distributions have been empirically measured in connection with UAPs, every assumption of very large synchrotron luminosities would be premature. Instead, a conservative upper bound of order L ~ 10-50 MW is adopted for the combined thermal/non-thermal contribution under strong confinement fields. In many scenarios, especially where the magnetic field is modest or plasma density is low, the non-thermal component may be negligible.

Now, consider a disc-shaped object surrounded by a plasma sheath of approximately 0.5 m thickness and embedded in a magnetic field of B ~ 100T. The observable flux at a distance is obtained from:

$$b = \frac{L}{4\pi d^2}$$

At a distance of d = 1 km, this corresponds to a flux of only b≈0.8-4W m^{-2}, well below the solar constant (~1360 W m^{-2}) but 500,000 times greater than Venus, and 1000 times brighter than the Moon (Maccabee 1999; Vallee 1998; Vallee *et al.* 2025; Fig. 2). Thus, even tens of megawatts of visible radiation would produce a bright but not overwhelmingly luminous source. In any fact, such an object would be sufficiently bright to allow high-resolution spectroscopy with short integration times and favorable signal-to-noise ratios (Jefferies and Mickey 1991; Landi Degl'Innocenti and Landolfi 2004; Teodorani, 2024).

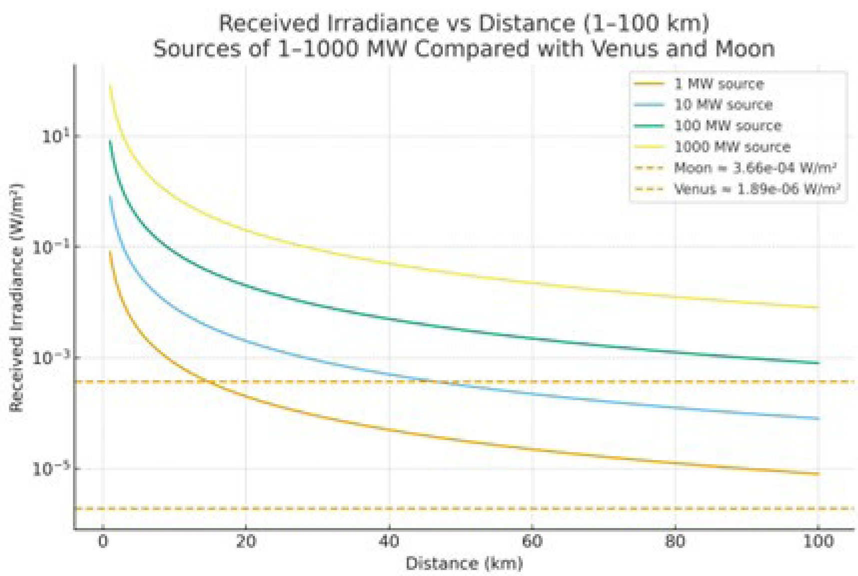

Figure 2. Received irradiance as a function of distance (1–100 km) for isotropic light sources with luminosities of 1, 10, 100, and 1000 MW. The curves show the expected dependence (assumed visible fraction f_{vis} = 0.1), plotted on a logarithmic scale to highlight the rapid decay of flux with distance. Horizontal dashed lines indicate the approximate irradiance of the Moon and Venus as seen from Earth, providing familiar reference levels. Even for sources radiating hundreds of megawatts, the received irradiance at tens of kilometers remains well below solar levels but can exceed that of Venus or the Moon depending on distance and luminosity.

If the magnetic field is weaker, *e.g.*, B~1 T, synchrotron emission is strongly suppressed unless the electron Lorentz factors satisfy $\gamma >> 10$. In such cases, the total luminosity is dominated by thermal emission and remains in the range of ~1-2 MW, governed primarily by temperature and density. Conversely, even extremely strong magnetic fields (up to B~1000 T) do not guarantee high luminosity: if the plasma density is low, the emissivity may be many orders of magnitude below a megawatt.

Even under extreme fields approaching 1000 T, if the plasma density is very low, the net luminosity remains negligible, many orders of magnitude below 1 MW. To achieve megawatt-scale luminosities, the plasma sheath must attain high radiative temperatures (Fig. 3).

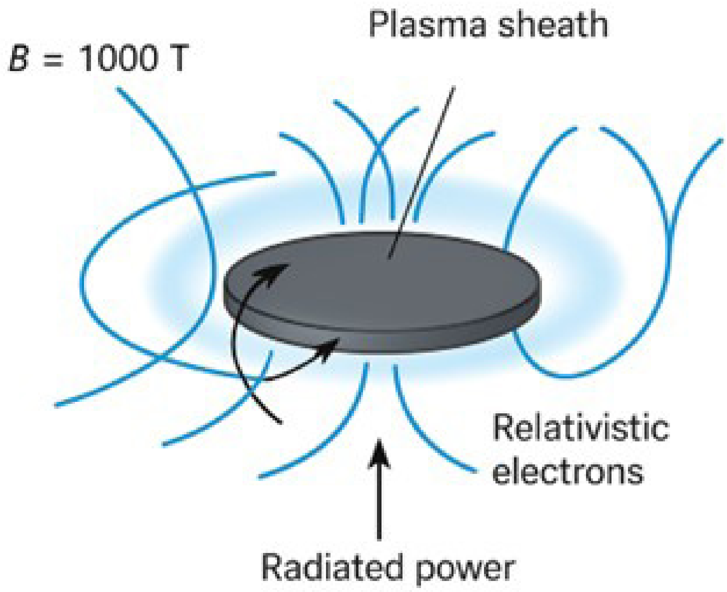

Figure 3. Configuration of a solid UAP surrounded by a magnetic field and a plasma sheath able to accelerate relativistic particles.

Now, to provide geometric scaling, we consider a disk of diameter 10 m, emitting from both sides. Its effective radiating area is:

$A = 2\pi r^2 = 157\ m^2$

Using $\varepsilon = 1$ (ideal upper bound, using $L = \varepsilon A \sigma T^4$), the corresponding thermal luminosities are:

$T = 1300$ K: $L_{th} \approx 25$ MW
$T = 2400$ K: $L_{th} \approx 295$ MW
$T = 4200$ K: $L_{th} \approx 2.8$ GW

Real plasma emissivities ($\varepsilon < 1$) or partial optical thickness would proportionally reduce these luminosities.

Regarding spectral characteristics, the peak wavelength of thermal emission for temperature T is given by Wien's displacement law:

$$\lambda_{\max} = \frac{2.90 \times 10^{-3}}{T}\ \mathrm{m}$$

Thus:

1300 K: $l_{max} \approx 2.2$ μm (near-IR)
2400 K: $l_{max} \approx 1.2$ μm (near-IR)
4200 K: $l_{max} \approx 0.69$ μm (red-visible)

Therefore, thermal emission at these temperatures produces infrared and visible radiation, but not X rays. Significant thermal X-ray emission requires temperatures in the range of 10^6-10^7 K, while non-thermal mechanisms (*e.g.*, highly energetic electrons) require independent spectroscopic confirmation.

In conclusion, it is possible to state this:

1. The corrected thermal luminosities for a 10 m disk at temperatures 1300-4200 K range from 25 MW to ~ 3 GW, assuming ideal blackbody emission.
2. Actual luminosities may be much lower if the plasma is optically thin or has emissivity $e < 1$.
3. Wien's law shows emission peaks in the infrared and visible, not in X-rays.
4. Irradiance at typical encounter distance (1-10 km) remains modest (1-100 W/m^2), consistent with bright but not hazardous appearance.
5. Radar and optical behavior depend on different physical parameters (electron density vs. temperature and emissivity) and are not in conflict.

It is important to note that although the magnetic field constrains plasma motion and accelerates charges, it does not itself perform mechanical work on the craft, and therefore does not directly contribute to its translational dynamics (Bellan 2006). The role of the magnetic field is to provide confinement and to accelerate particles within the sheath, producing synchrotron or cyclotron radiation as electrons spiral around magnetic field lines. These processes can dominate the luminosity if a sufficient population of relativistic charges is present (Bekefi and Barrett 1977).

The analogy to controlled fusion systems is again instructive. Plasma confinement in devices such as tokamaks and stellarators requires magnetic fields of 5–15 T, with advanced experiments exceeding 20 T (Chen 2016). Hypothetical technologies, potentially employing exotic superconductors or unconventional energy sources, could in principle generate hundreds or even thousands of tesla (Tajmar 2002). Fields of this magnitude are capable of confining plasmas with temperatures above 10^7 K, producing intense ultraviolet, X-ray, and microwave radiation, and generating sharp electromagnetic gradients in the surrounding environment (Bellan 2006; Peratt 1992).

If plasma temperatures reach ~ 10,000 K, luminosities may extend into the tens or hundreds of gigawatts (Vallee 1998). However, such hot plasma expands rapidly unless constrained. Without magnetic confinement or external pressure, a dense plasma shield in vacuum would disperse almost immediately, making long-lived free plasma configurations impractical. Stable plasma envelopes require continuous input of energy to compensate for losses, and confinement fields to prevent dissipation (Bellan 2006; Chen 2016). Observationally, the presence of strong magnetic fields can be detected through polarization measurements, magnetometric anomalies, or Zeeman splitting in spectral lines, with relative shifts that become increasingly significant in the radio and microwave domains (Jefferies and Mickey 1991; Landi Degl'Innocenti and Landolfi 2004; Stenflo 1994).

Finally, it is important to emphasize that high optical luminosity and radar-absorption or stealth behavior arise in distinct plasma regimes and therefore need not co-occur. The high-brightness cases discussed above correspond to hot, radiatively efficient sheaths or to populations of energetic particles, whereas radar-absorption and 'stealth-like' signatures require cooler, denser, and more weakly emitting plasmas that can strongly attenuate incident microwave energy. Thus, a UAP need not be simultaneously luminous and radar-absorbing; these behaviors represent different physical states of the plasma environment and cannot coexist under the same conditions. In other words, 'bright' and 'stealthy' behaviours correspond to different values of B, n_e, T, optical depth, and thus describe different physical states rather than a contradiction. This clarification removes the apparent tension between high-power scenarios and low-observability claims (see Section 5).

4. Magnetic Refraction

Plasma is an ionized gas consisting of free electrons and ions that responds strongly to electromagnetic fields and exhibits a variable refractive index (Chen 2016; Bellan 2006). When a UAP is enveloped in plasma and surrounded by an intense magnetic field, it can theoretically modify the propagation of electromagnetic radiation in its vicinity. Magnetic confinement of the plasma, analogous to techniques employed in fusion research such as tokamaks or stellarators, could stabilize such envelopes over extended periods (Bellan 2006).

The propagation of light through media with different refractive indices results in bending, or refraction. In a magnetized plasma, the refractive index becomes frequency-dependent and anisotropic due to the presence of the magnetic field (Ginzburg and Rukhadze 1972). This anisotropy can cause light rays to bend, split, or experience polarization rotation, as in the Faraday effect. Consequently, the visual appearance of a UAP may be distorted, shimmer, or even become partially invisible, depending on the observer's angle and the wavelength of the incident light (Tsakadze 1999; Bellan 2006). This phenomenology is found many times in UAP witness reports (Project Condign 2000).

While "magnetic refraction" is not a standard phenomenon in classical physics, the concept effectively describes the modification of the plasma's refractive index under strong magnetic fields. Ionized media exhibit refractive indices that depend on both electron density and the local magnetic field, and intense fields can alter plasma behavior dramatically, affecting the propagation of light and electromagnetic waves (Ginzburg and Rukhadze 1972; Kruer 1988). More precisely, these effects result in birefringence, in which electromagnetic waves split into ordinary and extraordinary modes with distinct propagation characteristics, producing beam bending, polarization rotation, or phase distortions (Stix 1992).

Observable optical effects from such a system may include pronounced light distortion (Fig. 4). A UAP surrounded by a plasma sheath and magnetic field could:

- Curve light around itself, producing unusual visual phenomena akin to mirages or blurred shapes.
- Act as a dynamically varying lens, where changes in plasma refractive index induce flickering, scintillation, or partial optical camouflage (Bellan

2006; Peratt 1992).

- In extreme cases, generate partial invisibility or active camouflage, depending on the light frequency and plasma behavior (Chen 2016).

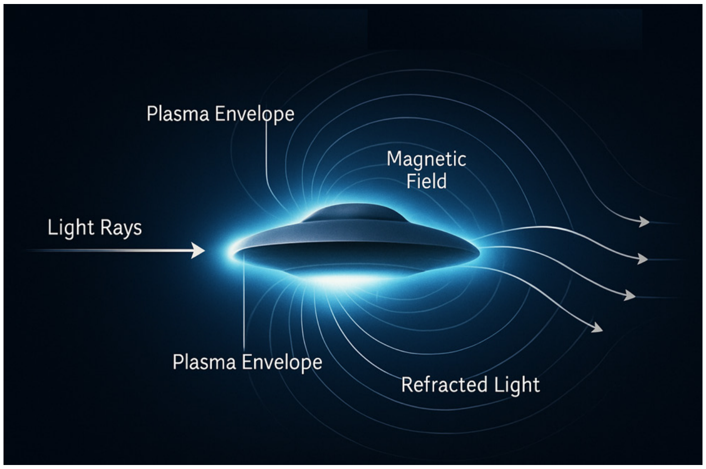

Figure 4. Sketch showing possible magnetic refraction effect from UAP.

Furthermore, the magnetic field can rotate the plane of polarization of transmitted light, resulting in apparent color shifts or anomalous polarization (Landi Degl'Innocenti and Landolfi 2004; Jefferies and Mickey 1991). Light originating from sources behind the object may appear displaced, distorted, or rotated relative to its actual position, reinforcing the potential for optical misperception.

Magnetic refraction may overlap with relativistic effects if a UAP employs a propulsion mechanism that warps spacetime (Knuth *et al*. 2019; Teodorani 2000). It is conceivable that both magnetic and warp-drive systems are employed—either simultaneously or in alternation—depending on flight requirements. Distinguishing between these two effects can therefore be challenging.

5. Zeeman Effect and Magnetic Field Strength

The Zeeman effect, first observed by Pieter Zeeman in 1896, refers to the splitting of atomic spectral lines under the influence of a magnetic field (Zeeman 1897; Griem 1974; Fig. 5). This effect plays a fundamental role in astrophysics, plasma diagnostics, and high-energy physics. The magnitude of spectral line splitting scales linearly with magnetic field strength and quadratically with the wavelength of the observed transition. Accurate detection of Zeeman splitting provides a direct method to measure magnetic fields in remote or extreme environments (Jefferies and Mickey 1991; Gray 2005; Wiley *et al*. 2007).

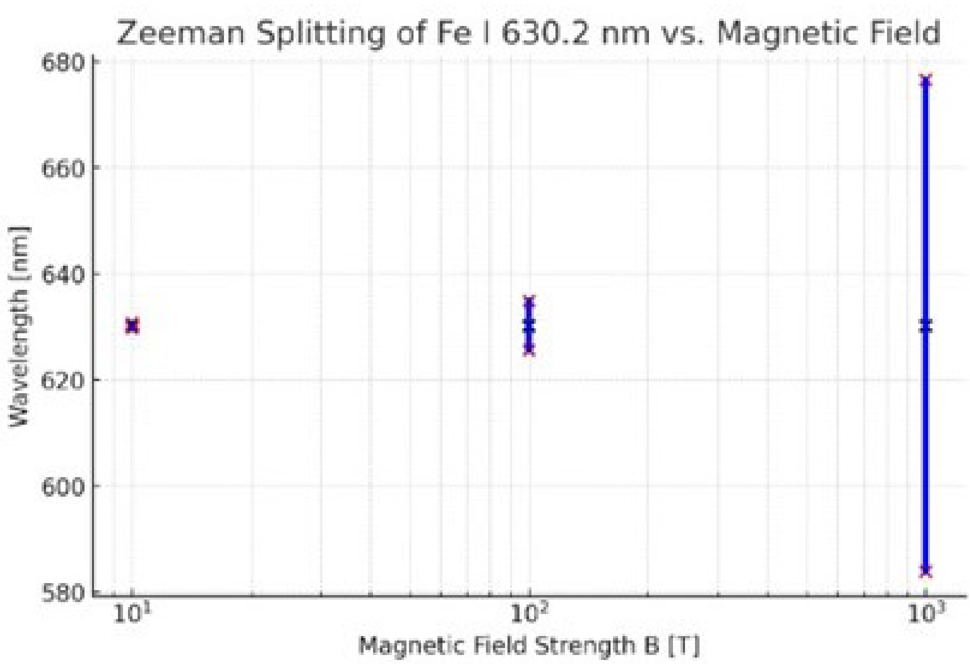

Figure 5. *Z*eeman splitting for Fe I 630.2 nm spectral line at magnetic fields of 10, 100, and 1000 T. Black dot: central unshifted wavelength λ_0. Red dots/lines: σ^+ and σ^- split components. X-axis: B in Tesla (log scale). Y-axis: wavelength in nm. The lowest field shown (0.0856 T) produces a splitting of 0.1 Å. Higher fields illustrate increasingly resolvable splitting. Note: 1 nm = 10 Å.

The observable splitting $\Delta\lambda_Z$ depends on the magnetic field *B*, the wavelength *λ* of the spectral line, and the intrinsic Landé factor *g* of the transition, which accounts for the splitting based on the total angular momentum quantum numbers of the energy levels involved. It is given by:

$$\Delta\lambda_Z = \frac{e\,\lambda^2\,g\,B}{4\pi m_e c}$$

This represents the classical linear Zeeman effect, where *e* is the elementary charge of the electron, *m* is the electron mass, *c* is the speed of light in vacuum, and *g* is the Landé factor. This formula allows direct estimation of the magnetic field strength from spectroscopic measurements.

Uniting together all the constants, the formula above can be expressed in practical units for astrophysical and laboratory applications, in this compact form:

$$\Delta\lambda_Z = 4.67 \times 10^{-13}\,\lambda^2\,g\,B$$

As an illustrative example, for Fe I 15648 Å spectral line ($\lambda = 1.5648\times10^{-6}$ m) and g = 2.5, this evaluates to $\Delta\lambda_Z \approx 2.86$ x (B/T). Thus a field of 0.1 T produces $\Delta\lambda \approx 0.286$ Å, and 1 T produces $\Delta\lambda \approx 2.86$ Å. At resolving power R the instrumental element width is $\Delta\lambda_{res} = \lambda/R$; for R = 50,000 at 15648 Å, $\Delta\lambda_{res} \approx 0.313$ Å. Hence fields B ≳ 0.1 T yield splittings comparable to a single resolution element and are detectable with R ≥ 50,000 and S/N ≥ 10–20 (see Table 3).

For a typical visible line at λ ≈ 5000 Å, assuming the normal Zeeman effect (g = 1), a splitting of $\Delta\lambda_Z = 0.1$ Å corresponds to a magnetic field of approximately:

$$B \approx \frac{4\pi m_e c\,\Delta\lambda_Z}{e\lambda^2 g} \approx 8.56 \times 10^{-2}\ \text{T}\ (85{,}600\ \mu\text{T})$$

For hypothetical UAPs with magnetic fields in the range of 1–10,000 T, optical and near-infrared spectroscopy provides particularly effective diagnostics (Landi Degl'Innocenti and Landolfi 2004; Table 1). The sensitivity of a given spectral line to Zeeman splitting increases with wavelength ($\Delta\lambda_Z \propto \lambda^2$), making infrared lines such as Fe I at 15648 Å far more responsive than optical lines like H_α at 6563 Å (Gray 2005; Rüedi *et al.* 1995). The splitting must exceed line broadening mechanisms (Griem 1974), such as Doppler and collisional effects, to be resolvable, defining a threshold field B_{thr}. For example, Fe I lines at 15648 Å and 6302 Å can show resolvable splitting with magnetic fields of a few hundred gauss, whereas shorter wavelength lines require fields of 0.1 T or higher (Jefferies and Mickey 1991).

The required spectral resolution R = λ / Δλ depends on the transition and the strength of the field. Infrared lines sensitive to the Zeeman effect typically require R ~ 10^3–10^4, whereas less favorable lines in the visible may demand R ≥ 10^5. In extreme environments such as a UAP plasma shield with *B* ~ 10–1000 T, the Zeeman splitting would be clearly resolvable for many transitions, making Zeeman spectroscopy a robust method to directly measure local magnetic fields (Landi Degl'Innocenti and Landolfi 2004; Teodorani 2024, Table 1).

B (T)	**$\Delta\lambda_Z$ (Å)**	**Comment**
0.0856	0.1	Minimal detectable splitting at 5000 Å, g = 1
1	1.17	Easily resolvable
10	11.7	Strong splitting
100	117	Extreme field scenario

Table 1.

A practical constraint is that the Zeeman splitting $\Delta\lambda_Z$ must exceed the Doppler and collisional broadening associated with the plasma temperature *T*. For instance, for hydrogen at $T = 10^5$ K, the Doppler FWHM at 5000 Å is approximately 0.56 Å. Thus, for B ≥ 10 T, Zeeman splitting surpasses the Doppler width, whereas for B ~ 0.1 T, high spectral resolution (R ≳10^4) and high signal-to-noise ratios are required. For fields on the order of 100–1000 T, resolutions R ≳ 10^3 are sufficient to resolve the splitting. For example, for B = 1000 T observing Fe I 6302 Å (g = 2.5), a resolution R ≳ 7000 is sufficient to resolve the Zeeman components. In plasma-shielded UAPs, Doppler and collisional broadening may partially obscure splitting, so high spatial resolution or modeling may be necessary to isolate the effect (Landi Degl'Innocenti and Landolfi 2004).

Certain spectral lines in the visible and near-infrared are particularly sensitive due to large Landé factors and suitable energy levels. These lines are commonly employed in astrophysics to measure magnetic fields in sunspots and active stellar regions and would serve similarly in diagnosing a magnetized plasma sheath around a UAP (Gray 2005; Jefferies and Mickey 1991; Table 2).

In several cases, even when the spectral dispersion is insufficient to resolve the two typical peaks (sometimes three) of the Zeeman effect, it is still possible to detect that the spectral line is anomalously broadened (with an unusually large FWHM) compared to a laboratory reference line. In such cases, the two unresolved Zeeman components merge into a single broadened structure, sometimes with two peaks on the very top of the line. Zeeman splitting can then be inferred through fitting models (Benedetto 1975) capable of reconstructing the underlying peaks while accounting for additional broadening contributions such as pressure/collisional and Doppler effects.

Element	Wavelength (Å)	Range
Ca II	3968, 3934	Visible
O II	4649, 4662	Visible
Hβ	4861	Visible
Mg I	5167, 5173, 5184	Visible
Fe I	5250	Visible
He I	5876	Visible
Na I – D1 & D2	5890, 5896	Visible
Fe I	6173, 6302	Visible
[O I]	6300, 6364	Visible
Hα	6563	Visible
O I	7770	Visible
Ca II	8498, 8542, 8662	Near Infrared
He I	10830	Near Infrared
Fe I	15648	Near Infrared

Table 2.

In most cases, acquiring spectra at high or even medium resolution ($R \sim 10^3$) requires relatively long integration times, typically ranging from several minutes to hours. This necessitates continuous tracking of the UAP using a Pan-Tilt-Zoom (PTZ) camera, while dispensing with the spectrograph slit to ensure optimal centering of the object and to greatly improve the tracking (at the cost of loss of resolution of about a factor 5) (Masters 2014). The requirement arises from the fact that such luminous phenomena generally exhibit brightness comparable to, or weaker than, that of Venus observed at night. Nevertheless, well-documented exceptions exist in which exceptionally bright UAPs ($100 \text{ MW} \leq L \leq 1 \text{ GW}$) permit the acquisition of high-resolution spectra with integration times of only a few seconds, yielding an adequate signal-to-noise ratio (Vallee 1998, 2025; Teodorani 2024). Under these conditions, it becomes possible to obtain multiple spectra during the visibility interval of the UAP, allowing investigation of temporal variability in the Zeeman effect and, consequently, in the associated magnetic field strength, should one be present. The most effective strategy for capturing such high-luminosity events remains the deployment of automated measurement stations.

In order to convert these qualitative considerations into a falsifiable framework, we express the Zeeman diagnostics in terms of explicit observational hypotheses with numerical bounds. For a spectral line of central wavelength λ, Landé factor g, and magnetic field B, the expected Zeeman separation is given by the standard relation:

$$\Delta\lambda_Z = 4.67 \times 10^{-13}\, \lambda^2\, g\, B$$

which provides a direct testable prediction. Let's now make a significant example. For the Fe I 15648 Å line – an especially sensitive near-infrared tracer with $g \sim 1.5 - 3$ – a coherent sheath field of $B \approx 1$ T produces a splitting of order $\Delta\lambda_Z \approx 2 - 3$ Å (see comparative values in Table 3). This far exceeds the expected thermal Doppler width ($\Delta\lambda_D \sim 0.05 - 0.15$ Å for $T = 10^3 - 10^4$ k), according to equation (m atomic mass of emitter, k_B Boltzmann constant, c light speed):

$$\Delta\lambda_\mathrm{D} \approx 2.355\, \frac{\lambda}{c} \sqrt{\frac{k_B T}{m}}$$

Such splitting is readily resolvable with a spectrograph of resolving power $R \gtrsim 6 \times 10^3$ and signal-to-noise ratio $S/N \gtrsim 50$. Therefore, a non-detection of Zeeman structure at this sensitivity would directly exclude any coherent magnetic sheath stronger than $B \geq 0.03 - 0.1$ T, once uncertainties in g, viewing geometry, and optical depth are taken into account. Conversely, measurement of resolved σ-components at the predicted separation would provide an unambiguous determination of B, independent of plasma density or temperature. This establishes a clear, observationally falsifiable hypothesis: the presence (or absence) of Zeeman splitting at the predicted level in Fe I 15648 Å or analogous high-g lines yields a quantitative constraint on UAP magnetic-field strengths within the emitting region.

Fe I 15648 Å (representative) — splitting and instrument R

B(T)	**$\Delta\lambda_Z$ (Å)**	**Required resolving power $R \geq \lambda/\Delta\lambda_Z$**
0.1	0.286	5.5×10^4
1	2.86	5.5×10^3
10	28.6	5.5×10^2
100	286	55

Thermal Doppler FWHM (Fe, λ=15648 Å)

T(K) Thermal FWHM	**$\Delta\lambda_D$ (Å)**	**Required resolving power $R \geq \lambda/\Delta\lambda_Z$**
1.0×10^3	0.0474	3.30×10^5
5.0×10^3	0.1061	1.48×10^5
1.0×10^4	0.1500	1.04×10^5

Table 3.

Let us now consider the quality of the actual observational data. Suppose we conduct spectroscopic observations of a UAP with four possible magnetic-field strengths, located at a distance of 10 km, using a spectrograph with resolving power R = 10,000. What signal-to-noise ratio could we achieve for each magnetic-field value? This allows us to assess the observational conditions under which scientifically meaningful results can realistically be obtained (see Fig. 6).

It is evident that a UAP with a strong magnetic field can be subjected to spectroscopic analysis far more effectively than one with a weak field, given that its luminosity—scaling approximately as $L \propto B^2$ under the assumption that the magnetic field and its confined plasma are the dominant radiative sources—decreases with the inverse square of distance. Under these conditions, the enhanced brightness improves the measurable Zeeman splitting in spectral lines (and therefore the inferred magnetic-field strength), as well as the detection of additional spectroscopic signatures such as

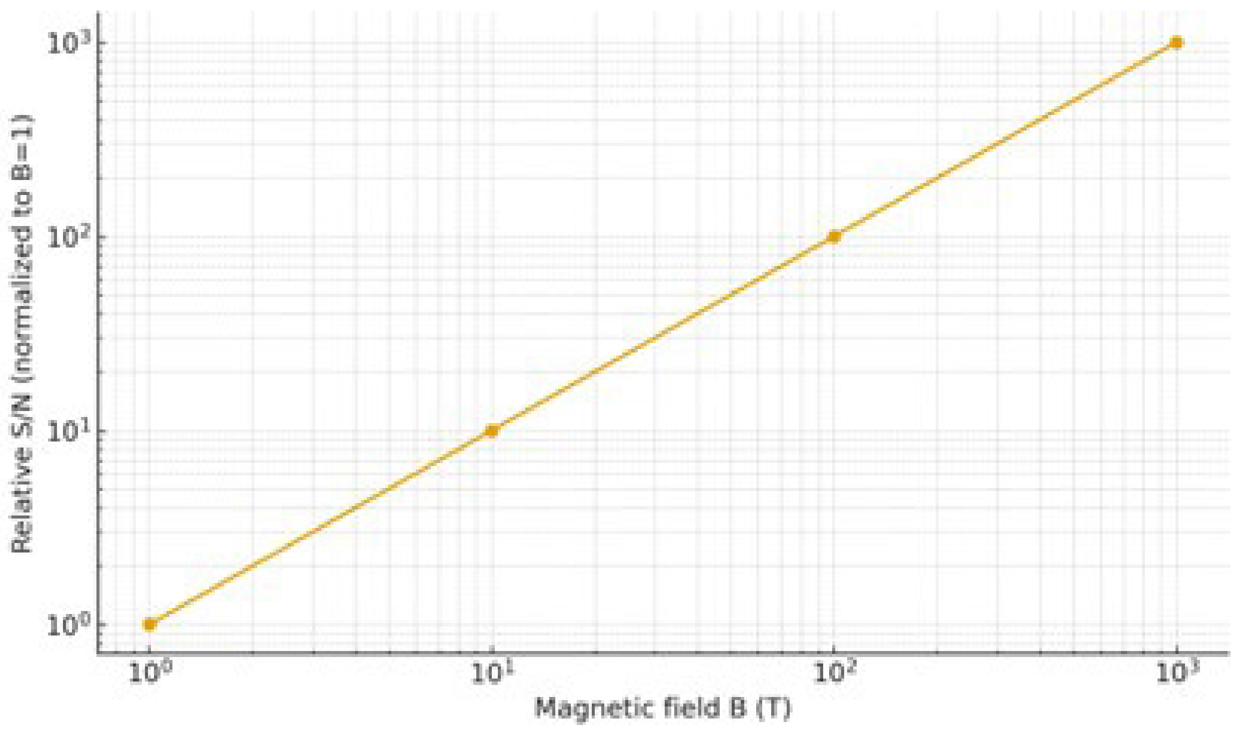

Figure 6. Relative signal-to-noise ratio (S/N) per spectral resolution element as a function of magnetic-field strength B for a fixed observation distance of 10 km and a spectroscopic resolving power of R = 10,000. The model assumes magnetoplasma emission with (absolute) luminosity scaling as $L \propto B^2$ and a shot-noise-limited detector regime, for which $S/N \propto \sqrt{(L/R)}$. With resolution held constant, this yields $S/N \propto B$. Values are normalized to the S/N obtained at B = 1. This plot illustrates the steep increase in detectability for higher magnetic-field strengths. Absolute S/N values depend on camera or telescope aperture, optical throughput, and exposure time and are not shown here.

Doppler shifts or elemental and ionic line identifications.

Alternatively, if the light source is weak (1–10 kW) and the UAP persists for a relatively long time (1–10 minutes), remaining stationary or moving slowly in a linear or slightly wobbling path, it becomes feasible to use long integration times by tracking the object with a Pan-Tilt-Zoom (PTZ) camera connected to a slitless spectrograph for improved tracking (see Masters 2014).

Simulations of possible scenarios are presented in some detail in Appendix A. Methodological issues are discussed also in Appendix B.

6. Interference with Radar and Laser

High-Power Microwave (HPM) and directed electromagnetic systems have the potential to induce transient disruptions in magnetically confined, plasma-encased objects. Energy coupling into the plasma shield may momentarily destabilize the field, creating transient openings or local emissions. However, in tightly regulated plasmas with strong magnetic confinement, the shield can adaptively absorb or deflect incoming energy, maintaining stability (Benford *et al.* 2007; Kruer 1988).

Historical reports provide anecdotal evidence consistent with such interactions. Notable UAP encounters, such as the 1976 Tehran incident and the Belgian Wave of 1989–1990, reported radar lock loss, avionics disruption, and erratic or intermittent radar signatures (Strand, 1984; Tedesco & Tedesco 2024), consistent with plasma-magnetic field interactions rather than conventional aircraft behavior (Greenewald 2025; Hendry 1979; Meessen 2011).

Historical reports provide anecdotal evidence consistent with such interactions: see Table 4.

Observational Method	**Anomalous Effect**	**Proposed Plasma/Magnetic Mechanism**
X/S-band Radar	Scattered or absent return	Reflection, refraction by plasma sheath
Pulsed Doppler	Incoherent velocities	Magnetoionic distortion
Microwave Beam	Plasma flare / temporary blackout	EM absorption or local instabilities
Phased Array Tracking	Shifting or ghost echo	Beam distortion due to plasma/magnetic gradient

Table 4.

Plasma and magnetic field configurations provide plausible physical mechanisms for many anomalous radar observations. Interactions between high-energy electromagnetic waves and these fields follow well-established plasma physics principles, including reflection, absorption, scattering, and propagation distortion (Chen 2016). Empirical investigation using multi-band radar and high-intensity directed energy sources could help validate these models.

Considering laser–plasma interactions, a confined plasma envelope subject to a strong magnetic field exhibits complex, nonlinear responses to incident electromagnetic radiation. The plasma's behavior is determined by electron density n_e, magnetic field strength B, field topology, and incident wave parameters. An electromagnetic wave can propagate only if its frequency ω exceeds the plasma frequency ω_p:

$$\omega > \omega_p = \sqrt{\frac{n_e e^2}{\varepsilon_0 m_e}}$$

where e is the electron charge, ε_o the vacuum permittivity, and m_e the electron mass. For $\omega < \omega_p$, the plasma acts as a reflective barrier; for $\omega > \omega_p$, partial penetration and absorption may occur (Bellan 2006; Chen 1984). Strong magnetic fields modify plasma response by inducing gyromotion, confinement along field lines, and anisotropic propagation, leading to phenomena such as Faraday rotation and mode-dependent wave behavior (Ginzburg and Rukhadze 1972).

The interaction of a high-intensity laser with a magnetically confined plasma envelope produces multiple effects:

- Reflection and partial absorption of incident beams.

- Scattering and redirection of energy along field lines.
- Localized heating and ionization enhancing plasma density temporarily.
- Nonlinear modulation of transmitted frequencies due to strong-field effects (Kruer 1988; Tsakadze 1999).

The confinement topology—whether toroidal, mirror, or custom—determines the plasma's stability and its interaction with incident beams. Extreme field strengths approaching 10^9 T could induce quantum electrodynamics (QED) effects such as vacuum birefringence, although such conditions are likely only in exotic astrophysical or hypothetical propulsion contexts (Adler 1971).

Overall, laser–plasma–magnetic interactions are governed by complex, nonlinear dynamics dominated by reflection, scattering, and absorption. The plasma sheath, controlled by magnetic fields, can adaptively respond to incoming electromagnetic energy, demonstrating behaviors that could account for anomalous radar or optical phenomena observed in UAP encounters. These theoretical scenarios align with established plasma physics principles and provide a framework for analyzing potential advanced propulsion or defensive shielding systems (Peratt 1992; Bellan 2006).

7. Interference with Aircraft Equipment

Alleged UAP have frequently been reported to generate strong electromagnetic fields and plasma-like envelopes, capable of interacting with nearby electronic systems and human operators. Empirical and anecdotal evidence from military, civilian, and declassified reports indicates a consistent pattern of electromagnetic interference (EMI), instrument disruption, and optical anomalies (ODNI 2021; Project Condign 2000). This section synthesizes these observations and evaluates their physical plausibility in terms of electromagnetic theory and plasma physics.

Electromagnetic and Plasma-Induced Effects

When a UAP with a high-intensity magnetic field (B~100 T) and a confined plasma envelope approaches an aircraft, multiple phenomena may occur depending on distance and field intensity:

1. Electromagnetic Interference (EMI)
   - Strong magnetic fields can perturb onboard electronics, avionics, radar, radio, GPS, and autopilot systems.
   - Temporary instrument malfunctions or full blackouts are theoretically possible, analogous to directed-energy electromagnetic disturbances (Giri & Tesche 2004; Kaiser 2004).
2. Induced Currents
   - Time-varying magnetic fields may induce parasitic currents in conductive aircraft structures, generating local heating, sparks, or damage to electronic systems (Jackson 1998; Chen 2016).
3. Radar and Optical Distortions
   - Confined plasma envelopes can refract, absorb, or scatter radar waves, resulting in radar invisibility or erratic signatures (Ginzburg and Rukhadze 1972).
   - Optical distortions include glowing auras, shimmer, or apparent mirages caused by ionized gases and electromagnetic lensing.
4. Aerodynamic Perturbations
   - Plasma sheaths can locally alter air pressure or turbulence, potentially affecting airflow, causing vibrations, or inducing flight instability.
5. Instrument Anomalies
   - Magnetic compasses may behave erratically.
   - Attitude indicators, altimeters, and autopilot systems may report spurious readings.
   - Effects can resemble those caused by solar storms or electromagnetic pulses (EMPs) (ICNIRP 2020).
6. Digital System Vulnerability
   - Extremely strong fields could induce software crashes, resets, or data loss in sensitive electronics.
7. Pilot Physiological Responses
   - Exposure to high-intensity EM fields may cause disorientation, vertigo, nausea, or altered time and space perception, consistent with some anecdotal pilot reports (Glover *et al.* 2007; Persinger 2001).

Historical and Documented Incidents

Several well-documented cases illustrate the potential effects described above (Table 5). For instance, pilots during the Belgian Wave (1989–1990) reported sudden loss of instrumentation, visual disturbances, and apparent interference with flight control systems (Haines 2000; NICAP 1964; Project Condign 2000). Similar phenomena were reported during the 1976 Tehran incident, with radar and avionics disruptions concurrent with UAP observations (Greenewald 2025).

Effect Type	Mechanism	Observational Evidence
Electromagnetic interference	B-field coupling	Instrument anomalies, GPS disruption
Induced currents	Faraday induction	Heating, sparks in metal structures
Radar distortion	Plasma reflection/ scattering	Ghost targets, sudden radar loss
Optical distortion	Refractive bending	Glowing auras, mirage effects
Aerodynamic perturbation	Plasma-air interaction	Aircraft vibrations, turbulence
Digital system impact	Induced currents	Software crashes, data loss
Pilot physiological response	EM field exposure	Vertigo, nausea, hallucinations

Table 5.

The convergence of electromagnetic interference, induced currents, radar distortion, and pilot physiological effects suggests a reproducible and scientifically plausible pattern. A UFO with strong magnetic fields and/or a plasma envelope could generate substantial electromagnetic and plasma-induced effects on nearby aircraft, potentially mimicking directed-energy weapon impacts or large-scale electronic disruption. While the exact nature of these objects remains speculative, the documented observations support continued scientific and operational investigation (ODNI 2021; Peratt 1992; Bellan 2006).

Some of these effects have been documented – as EM interference – many times also when electric or electronic equipment on ground (including vehicles) are affected by the close proximity with a UAP (Rodeghier 1981).

8. Physiological Effects

Unidentified Flying Objects (UFOs) are frequently described as generating extremely strong electromagnetic fields, often associated with confined plasma envelopes. Exposure to such intense magnetic fields, potentially on the order of tens to hundreds of tesla, can have significant physiological consequences for humans (Glover *et al.* 2007; Persinger 2001). Drawing upon evidence from MRI studies, industrial high-field environments, and plasma confinement devices such as tokamaks (Chen 2016; Schenck 2000), it is possible to extrapolate the likely effects on neurological, neuromuscular, sensory, and psychological systems, as well as potential risks from plasma-derived radiation (WHO 2006, Table 6).

– *Neurological and Sensory Effects*

Strong static magnetic fields above approximately 3 T are known to produce vertigo, nausea, disorientation, and distorted perception of time, primarily through Lorentz forces acting on the conductive fluids in the semicircular canals of the inner ear (Glover *et al.* 2007; Schenck 2000). If the magnetic field varies in time, as might occur in pulsed plasma stabilization or oscillating propulsion systems, induced currents in the body according to Faraday's law can stimulate peripheral nerves and muscles, causing involuntary contractions, paresthesia, spasms, and in extreme cases, cardiac arrhythmias or neurological disruption (Reilly 1998; ICNIRP 2020).

– *Electromagnetic Radiation Effects*

Concomitant exposure to electromagnetic radiation emitted by the plasma, particularly in the infrared, ultraviolet, and X-ray ranges, can produce thermal injuries, corneal damage, cataracts, or even systemic effects in the presence of ionizing components (ICNIRP 2013; Hershcovitch 1995).

– *Cognitive and Psychological Effects*

Cognitive and psychological effects are also plausible; patterned electromagnetic exposure to temporal lobes has been associated with auditory or visual hallucinations, altered consciousness, and sensations of presence, potentially providing a mechanism for the "mystical" experiences often reported during close encounters (Persinger 2001, 2002).

– *Risks to Implanted Devices*

Strong fields may interfere with implanted electronic devices such as pacemakers or neurostimulators, and even passive metallic implants may move or heat under extreme exposure (Schenck 2000; Shellock 2002).

Effect Type	Mechanism	Observational/Experimental Evidence
Vertigo, disorientation	Lorentz forces on inner ear fluids	MRI, high-field lab exposures (Glover *et al.* 2007)
Nausea, vomiting	Induced currents in neuromuscular tissues	Plasma exposure models, Faraday law effects (Reilly 1998)
Involuntary muscle contractions	Time-varying B-fields	Industrial high-field studies
Cardiac arrhythmias	Induced currents, neurological disruption	Tokamak exposure simulations
Hallucinations, altered perception	EM interaction with temporal lobes	Neuropsychiatric case studies (Persinger 2001)
Thermal injury	IR/UV/X-ray radiation	Laser-induced plasma spectroscopy studies (Alfieri *et al.* 2020)
Implant interference	Induced currents in devices	MR safety literature (Schenck 2000; Shellock 2002)

Table 6.

Hypothetical Clinical Scenario

A hypothetical clinical scenario might involve an individual approaching within 20 meters of a UAP emitting a localized field exceeding 20 T, leading within one minute to vertigo, vomiting, hallucinations, burns, arrhythmias, and temporary cognitive deficits, with partial recovery over days to weeks.

These considerations indicate that any human exposure to a UAP with strong magnetically confined plasma would be physiologically hazardous, producing a characteristic set of acute and possibly chronic symptoms. Integrating plasma physics, high-field bioeffects, and neuropsychology provides a scientifically plausible framework for understanding the human impact of such extreme phenomena (ICNIRP 2020; Persinger 2001; Reilly 1998). This multidisciplinary approach also suggests that physiological effects can serve as diagnostic markers in close encounter investigations, complementing electromagnetic and optical measurements.

9. Warhead Power Against UAP

The minimum energy required to overcome a magnetically confined shield around a UAP has been estimated as $E_B \approx 3.98 \times 10^{11}\,\mathrm{J} = 398\,\mathrm{GJ}$ (Cooper 1996; Jackson 1998). Surpassing this energy threshold would theoretically require at least a tactical nuclear warhead (> 0.1 kilotons of TNT) or a high-energy directed pulse (such as lasers, particle beams, or railguns) capable of delivering hundreds of gigajoules in a very short time.

For a magnetic field of $B = 1000\,\mathrm{T}$, the hot plasma surrounding the craft could vaporize projectiles or deflect them if it has sufficiently high density, while the magnetic field itself can deflect charged particles, rendering many conventional weapons ineffective (Bellan 2006; Chen 2016). Moreover, the craft might absorb part of the incoming energy, further reducing the effectiveness of explosions. In such scenarios, magnetically shielded craft with fields ≥ 1000 T may be effectively immune to conventional kinetic or chemical-energy weapons and would require directed energy or nuclear-grade yields for neutralization.

a. *Magnetic Pressure vs. Thermal Pressure*

Considering the given object parameters, magnetic pressure dominates, while the thermal pressure caused by the impacting explosion is orders of magnitude smaller. The physical feasibility of neutralizing a UAP protected by a static magnetic field of 100 T raises fundamental questions in applied physics, ballistics, electromagnetism, and military engineering.

The situation can be concisely expressed by the following inequality, where the term on the left represents the magnetic pressure and the term on the right corresponds to the thermal pressure generated by a chemical explosion:

$$\frac{B^2}{2\mu_0} > n\, k_B\, T$$

where B is magnetic field strength, T the plasma temperature, μ_0 is the vacuum permeability, n is the particle numer density and k_B is the Boltzmann constant,

An analysis of using a 100 kg TNT explosive against a target enclosed by such a magnetic field includes interactions between the magnetic field and the projectile, Lorentz forces on conductive materials, attenuation of the shockwave, and potential electronic interference (Cooper 1996).

b. Lorentz Force on a Conductive Projectile

Assuming a uniform static field of B = 100 T along the z-axis, a metallic projectile or missile moving through this field experiences a Lorentz force:

$$\vec{F} = q(\vec{v} \times \vec{B})$$

For a neutral but conductive body, eddy currents are induced according to:

$$\vec{J} = \sigma(\vec{E} + \vec{v} \times \vec{B})$$

where σ is the electrical conductivity.

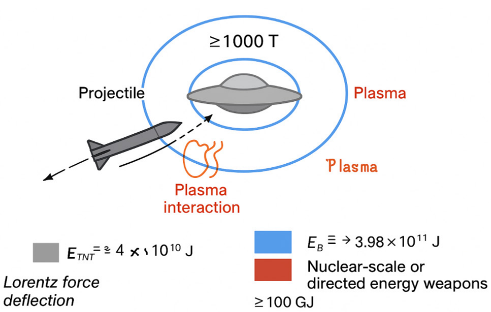

Figure 7. Comparison between a strongly magnetized UAP and an impacting kinetic or chemical weapon.

These currents produce Joule heating:

$$P = \int \vec{J}^2/\sigma \, dV$$

and resistive torques that slow down or deflect the missile. The energy released by 100 kg of TNT is approximately (Fig. 7):

$$E_{\mathrm{TNT}} \approx 4.184 \times 10^8\ \mathrm{J/kg} \times 100\,\mathrm{kg} = 4.184 \times 10^{10}\ \mathrm{J}$$

The resulting overpressure at a distance r can be estimated using standard blast equations (Cooper 1996).

For significant structural damage to an advanced metallic craft with magnetic shielding, the explosive must detonate within 2–3 meters. Due to the combination of magnetic deflection and plasma effects, the probability of success for a conventional 100 kg TNT charge is low, suggesting that non-conductive projectiles or directed-energy weapons would be more viable alternatives (Benford *et al*. 2007; Kruer 1988).

This analysis indicates that conventional kinetic or chemical munitions are unlikely to neutralize a magnetically shielded craft, emphasizing the need for high-energy, precision-directed solutions or nuclear-scale yields to overcome such advanced defenses. Theoretical considerations of magnetic shielding, plasma density, and energy absorption provide a quantitative framework for assessing the feasibility of countermeasures against UAP exhibiting extreme electromagnetic properties, as well as posing a threat.

10. Multimodal Instrumentation Platform

Unidentified Aerial Phenomena (UAP) have increasingly been documented under conditions consistent with strong localized magnetic fields and plasma envelopes, suggesting that these phenomena may involve high-energy processes with measurable electromagnetic, optical, and physiological effects (Peratt 1992).

This section presents a multimodal sensing platform designed to provide reproducible and peer-validated data by integrating magnetometric, spectroscopic, radiofrequency, and biological monitoring within a synchronized, portable system. The architecture is conceived to be mobile-capable and scalable, allowing field deployment in diverse observational contexts.

– System Architecture

Central to the design is the synchronization of heterogeneous sensors through GPS-based timing, ensuring cross-domain data comparability with nanosecond precision (Teodorani 2024; Fig. 8). The platform incorporates:

- Triaxial magnetometers for high-sensitivity magnetic field measurements.
- VLF-ELF and VHF-UHF spectrometers.
- Software-defined radios (SDRs) for broadband RF analysis.
- Optical cameras (all-sky, zoom and high-speed).
- FLIR thermal imager.
- Optical spectrometers capable of resolving Zeeman-split spectral lines.
- Optional biomedical modules for EEG and ECG recording.

– Measurement Protocol

The measurement protocol is based on trigger conditions designed to discriminate natural background from anomalous activity, including:

- Sudden magnetic field excursions exceeding 50 μT.
- Broadband RF emissions above −10 dBm.
- Rapid optical intensity changes greater than 5 lux per millisecond.
- Anomalous Doppler shifts or physiological responses (Glover *et al*. 2007).

Each measurement is precisely timestamped using GPS 1PPS signals with ±100 ns accuracy, ensuring that events detected by different subsystems can be correlated through convolution-based analysis.

Regarding the timing and robustness of the system, we must note that GPS timing can be disrupted by intense electromagnetic interference or ionospheric disturbances. For robustness we therefore recommend a redundant timing architecture: (i) GPS-disciplined oscillators (GDSOs) with hold-over using internal Rubidium oscillators to bridge short GPS outages; (ii) periodic cross-checks against terrestrial time signals (*e.g.*, WWV/DF or LTE/NTP time servers when available); (iii) a 1PPS radio beacon or optical sync flash recorded by all imagers as a backup time fiducial; and (iv) post-processing cross-correlation between independent sensors (optical flashes, magnetometer transients) to detect and correct residual offsets. These measures reduce the risk of false correlation due to transient GPS perturbations. Because GNSS timing may degrade under strong EM environments, we recommend redundant timing via GPS-disciplined rubidium oscillators and local precision protocols (*e.g.*, White Rabbit) to maintain < 1 μs synchronization across all stations.

All sensors are controlled through a modular acquisition framework built on Python, Raspberry Pi, and GPS/NTP-synchronized triggers, allowing the integration of diverse measurement modalities.

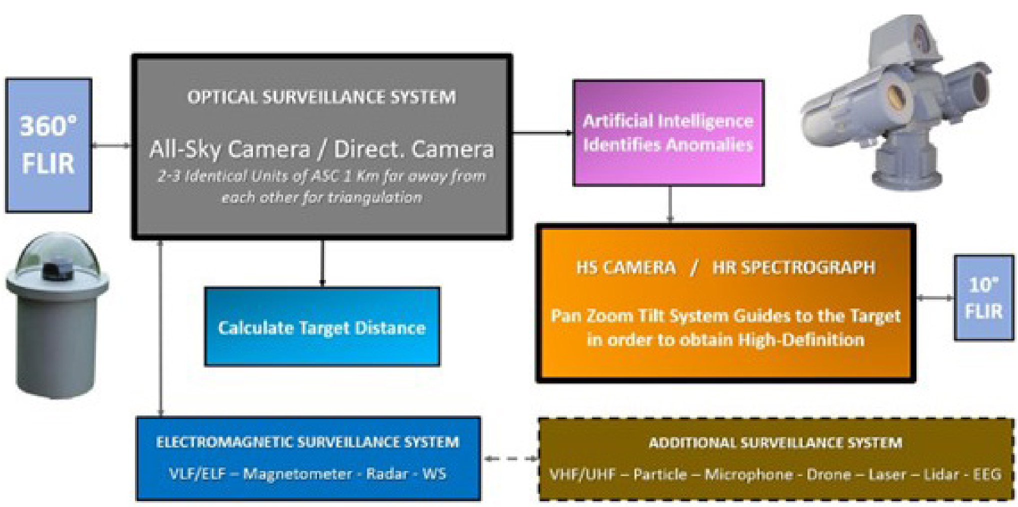

Figure 8. Flowchart illustrating a sample procedural measurement protocol proposed by the author. The setup includes: all-sky cameras, a VLF–ELF spectrometer, a microwave spectrometer, a magnetometer, a weather station (WS), a pan–tilt–zoom camera, a FLIR thermal imager, a high-resolution optical spectrometer, a high-speed camera, a particle detector, a microphone, a laser, a lidar system, and an EEG device. Additionally, the use of a drone is anticipated to approach UAPs when feasible.

– *Data Analysis and Optical Diagnostics*

Cross-sensor analysis enables identification of coherent signatures across electromagnetic and biological domains, reducing false positives caused by environmental noise. Optical diagnostics are enhanced by Zeeman-splitting analysis, where shifts in spectral lines, such as the hydrogen Hα transition, are quantified. Simulated values show that fields as low as 0.86 T yield splittings of 0.1 Å, resolvable with spectrometers of resolving power $\lambda/\Delta\lambda > 10^4$ (Jefferies and Mickey 1991; Teodorani 2024). Simulations of possible scenarios are presented in some detail in Appendix A. Methodological issues are discussed also in Appendix B.

– *False-positive controls and automated vetting*

To limit false positives we intend to adopt an automated multi-filter procedure: (1) cross-match observed track ephemerides with publicly available catalogs (NORAD/TLE, CelesTrak) to exclude satellites and rocket bodies; (2) use aircraft ADS-B feeds where available to remove known aircraft; (3) compare optical tracks with database of Iridium and other satellite flare geometries (*e.g.*, Heavens-Above models) and flag expected flares; (4) use a machine-learning classifier (trained on labelled examples of satellites, aircraft, meteors, and drones) to flag unusual signatures for human review; (5) require multi-modal confirmation (optical + magnetometer or optical + RF) before promoting an event to the "candidate" list. Code and training datasets are expected to be provided in the online repository to enable reproducibility.

– *Preliminary Numerical Simulations*

Numerical simulations using COMSOL Multiphysics suggest that plasma envelopes of density $n_e = 10^{17}\,m^{-3}$ and temperature $T = 10^4\,K$ produce measurable scattering signatures in both radiofrequency and visible spectra. These results are consistent with reported radar anomalies and optical distortions (Bellan 2006; Chen 2016).

– *Machine Learning Integration*

Machine learning methods, including density-based clustering (DBSCAN) and anomaly isolation (Isolation Forest), are employed to identify correlated deviations across multiple sensors, creating an adaptive analytic framework capable of detecting rare or transient phenomena (Watters *et al*. 2023) that escape conventional statistical approaches.

– *Physiological Monitoring (practical and ethical considerations)*

The integration of physiological monitoring is justified by reports of transient neurological and cardiac effects in proximity to UAP. Strict adherence to ethical protocols is maintained, including informed consent and passive, non-invasive monitoring, with active emissions limited to certified Class IIIB laser standards (Glover *et al*. 2007; ICNIRP 2013, 2020, Teodorani 2025).

For continuous ambulatory monitoring we propose using commercially available, medical-grade wearable devices (*e.g.*, wristband biometric monitors) that record heart rate, heart-rate variability, skin conductance, and peripheral temperature with minute-to-minute resolution. Use of full EEG is reserved for controlled studies with informed consent and with clear ethical approval; continuous, population-wide EEG monitoring is not proposed. All physiological monitoring is intended to follow institutional review board (IRB) protocols and data-protection rules (GDPR where applicable).

– *Laser/Lidar usage clarification*

If "*active emissions*" are used to observe the phenomenon, this refers to range-finding or lidar pulses for distance measurement and profiling (Class 1–3R eye-safe lidar is preferred). Any active laser use must comply with IEC 60825 laser-safety standards and should be operated only by certified personnel. The *Class IIIB* option is removed unless a device of that class is explicitly employed; if a Class IIIB system is used, its safety procedures and required approvals must be clearly documented. Any active optical probing—if used at all—must be restricted to Class I or II eye-safe devices.

– *Significance*

The broader significance of this approach lies in its ability to transition UAP research from anecdotal and fragmented reporting toward systematic, replicable measurement science. By combining electromagnetic diagnostics, optical spectroscopy, radiofrequency analysis, and physiological monitoring in a synchronized multimodal framework, the system provides a reproducible methodology deployable by civilian, academic, or defense institutions.

The data generated offer a means of testing hypotheses regarding plasma confinement, magnetic shielding, and anomalous radiation, providing a foundation for comparative studies across independent research groups. This convergence of precision sensing, computational analysis, and field portability establishes a baseline for future large-scale observational networks, advancing the empirical study of aerial anomalies from speculation toward a rigorous scientific domain (Teodorani 2024; Watters *et al.* 2023).

Initiatives of this kind were attempted in the past (Rutledge 1982; Strand 1984) and are still being carried out today (Watters *et al.* 2023).

11. Ground-Interaction Regime

When a magnetoplasmadynamic UAP descends and makes contact with the terrestrial surface, the coupled plasma–magnetic system undergoes a rapid reconfiguration. The collapse or modulation of its confining sheath produces measurable physical and chemical signatures that may persist in the local environment. These phenomena are not only of theoretical interest but also provide the most accessible empirical pathway for scientific verification.

– *Thermal and Chemical Effects*

The sudden recombination of ionized plasma species, together with transient Joule heating from induced currents, can deposit substantial thermal energy into the substrate. Documented cases of anomalous vitrification of soil and silicate fusion have been experimentally reproduced in fulgurite formation, where discharges produce glass-like structures and melting textures (Çalışkanoğlu *et al.* 2023). Vegetation exposed to such processes may exhibit scorched or dehydrated tissue, sometimes arranged in concentric or elliptical patterns consistent with field confinement geometries. Analytical methods such as X-ray diffraction (XRD) and differential scanning calorimetry (DSC) can reveal phase transitions and crystallographic changes induced by heating, while recent studies also show that plasma–surface interactions can transiently cool or otherwise alter thermal balances (Tomko *et al.* 2022). These are proposed only as ancillary environmental tracers, not as diagnostic signatures.

– *Magnetic and Electrical Signatures*

A plasma sheath confined by fields on the order of tens to hundreds of tesla would strongly interact with ferromagnetic and conductive ground materials. The rapid collapse of such fields at touchdown can imprint localized remanent magnetization or, conversely, demagnetize susceptible minerals. Comparable phenomena have been observed where volcanic ash exposed to lightning displayed significant magnetic alterations (Genareau 2019). This effect is measurable using portable fluxgate or proton magnetometers, with anomalies often extending several meters beyond the apparent landing trace. Changes in soil conductivity and permittivity may also result from implanted ions and altered mineral chemistry, detectable with resistivity meters and ground-penetrating electromagnetic sensors.

– *Radiological and Atmospheric Traces*

Short-lived radiation signatures may accompany plasma–ground interaction. Lightning discharges are now known to trigger photonuclear reactions, producing neutrons and radioisotopes detectable in situ (Enoto *et al.* 2017; Wada *et al.* 2020). Such effects may contribute to weak gamma-ray emission, transient activation of soil constituents, or elevated atmospheric concentrations of ozone and nitrogen oxides. Controlled plasma jet studies confirm the efficient generation of O_3/NO_X at atmospheric pressure (Schütze *et al.* 1998; Harris *et al.* 2024). These phenomena can be monitored with gamma spectrometry, ion counters, and ozone analyzers. While most of these effects decay within hours, careful time-resolved monitoring can capture them.

– *Biological Alterations*

The surrounding biota can serve as sensitive indicators of landing events. Vegetation often displays chlorophyll degradation, necrosis, or anomalous fluorescence spectra consistent with exposure to elevated ultraviolet and microwave fields. Laboratory studies with atmospheric-pressure plasmas show that exposure induces intracellular ROS accumulation leading to plant cell death (Seol *et al.* 2017). At the same time, plasma-derived reactive species (RONS) are well-documented to trigger redox stress in biological systems (Privat-Maldonado *et al.* 2019). ROS (Reactive Oxygen Species) and RONS (Reactive Oxygen and Nitrogen Species) refer to chemically reactive molecules that can be produced in biological tissues under oxidative or electrophysical stress (*e.g.*, high UV or microwave exposure). Reported vegetation effects (chlorophyll degradation, necrosis) attributed in the literature to elevated ultraviolet and microwave exposure are case-dependent

(Sharma *et al*. 2010). These biological signatures are not presented as evidence of UAP but as routine biosurveillance markers commonly used in EM-exposure assessment. Soil microbial populations may also be significantly perturbed; work on disturbance ecology shows that major thermal/chemical transients (such as fire) reorganize plant-associated microbiomes and soil microbial assemblages (Dove *et al*. 2021). These bioindicators can be assessed using chlorophyll fluorometry and microbiological assays, respectively.

– *Persistence and Temporal Evolution*

The duration of detectable signatures is highly variable. Ionization-related effects vanish within minutes to hours, thermal and vegetative anomalies last days to weeks, while magnetic and mineralogical modifications can persist indefinitely, serving as long-term "fossil evidence" of the interaction. Phosphorus redox anomalies in fulgurites, for example, remain preserved geochemically over geological timescales (Pasek *et al*. 2009). Accordingly, any rigorous field investigation should combine rapid-response atmospheric sensing with longer-term geophysical and geochemical surveys.

12. Conclusions

This study has presented a comprehensive, physics-based framework for investigating Unidentified Aerial Phenomena (UAP), integrating advanced concepts from plasma physics, magnetohydrodynamics, high-field electromagnetism, spectroscopy, and bioelectromagnetics. A particular technical focus has been devoted to the photometric aspect and to the spectroscopic analysis in the optical and IR bands, followed by a more descriptive—yet fairly comprehensive—overview of observational techniques at other wavelengths and in different modalities. As can be seen in the final sections, this broad discussion is intended to provide a clear understanding of the problem at hand, so as to better determine how to acquire accurate data in the near future for optimal problem solving, using an automated multi-instrument station.

Due to the elusive and unpredictable nature of the phenomenon, the data collected in previous studies (Knuth *et al*., 2019; Maccabee, 1994, 1999; Meessen, 2012a, 2012b; Nolan *et al*., 2022; Rutledge, 1982; Strand, 1984; Tedesco & Tedesco 2024; Teodorani, 2004; Vallée, 1998, 2025 *et al*.) remain inevitably fragmentary. Some of these data comprise direct instrumental measurements—some of which were carefully calibrated—while others consist of indirect observations recorded by experienced personnel. Additionally, there are many highly detailed witness and anedoctal reports provided by both civilian and military observers.

The reality of the UAP field is that, at present, the overwhelming majority of available information is observationally anecdotal, heterogeneous in quality, and often lacking instrumented measurements. This is precisely the core motivation for the present work. This paper argues that the epistemic weakness of the existing record *requires* the construction of a rigorous, instrument-based framework capable of replacing anecdotal reports with reproducible scientific data, using (possibly) an automated (fixed or mobile) measurement station. Therefore, anecdotal references appear only as contextual indicators of recurrent features (*e.g.*, luminosity changes, sudden accelerations, radar intermittency) that are *commonly claimed* but remain untested. They serve not as evidence but as prompts for formulating testable hypotheses and defining instrument requirements.

Therefore, regarding all this it must be emphasized that:

1. Anecdotal descriptions are not treated as empirical facts, but as targets for falsification.
2. Each alleged phenomenon is intended to be translated into a quantitative, falsifiable prediction (*e.g.*, measurable Zeeman splitting above a given threshold; specific radar-cross-section variability; constraints on magnetic-field strengths and plasma parameters).
3. The proposed observational platform is designed specifically to validate or refute these claims through multi-instrument, time-synchronized acquisition.
4. Appendices A and B explicitly outline null experiments, calibration procedures, and simulated scenarios, illustrating how anecdotal elements become formal hypotheses to be tested—and likely rejected—under controlled conditions.
5. The goal is not to accept anecdotal reports but to remove the field from anecdotal dependence by establishing a replicable methodology.

Thus, the citation of anecdotal material in this paper is programmatic rather than evidential: it highlights exactly why the field requires a physics-based framework, why controlled measurement is necessary, and which specific claims require verification or dismissal. But without a fully scientific treatment of the problem, anecdotal reports are not science. Nevertheless, without acknowledging their existence, one cannot rationally design the experimental tools needed to move beyond them.

In summary, everything discussed in the preceding sections can be distilled into the following fundamental aspects, which should be subjected to scientific investigation:

1. **Plasma-Solid Differentiation:** Distinguishing between pure plasma phenomena and solid objects enveloped in plasma is achievable through combined diagnostics—spectroscopic, magnetometric, radar, thermal, and kinematic observations. The presence of a continuous thermal spectrum, coherent magnetic fields, sharp radar reflections, and stable motion strongly indicates a solid core within a plasma envelope (Peratt 1992; Teodorani 2024).
2. **Luminosity and Magnetic Effects:** The luminosity of UAPs is highly dependent on plasma temperature, density, and magnetic field strength. Extreme magnetic confinement can produce synchrotron and thermal Bremsstrahlung emissions detectable in visible, ultraviolet, and X-ray ranges. Observable brightness and color shifts provide practical avenues for remote sensing and Zeeman spectroscopy (Jefferies and Mickey 1991; Bellan 2006).
3. **Magnetic Refraction and Optical Distortions:** Plasma-magnetic field interactions can produce refraction, birefringence, polarization rotation, and apparent invisibility effects. These mechanisms offer plausible explanations for reported visual anomalies, shimmering effects, and partial optical camouflage observed during UAP encounters (Ginzburg and Rukhadze 1972).
4. **Electromagnetic and Physiological Interference:** Strong magnetic fields and confined plasma can disrupt aircraft electronics and human physiology, inducing vertigo, nausea, instrument anomalies, and temporary cognitive effects. This validates pilot and eyewitness reports and underscores the importance of including biological monitoring in observational studies (Glover *et al.* 2007; Persinger 2001).
5. **Resilience Against Conventional Weaponry:** Theoretical analysis suggests that magnetically shielded craft could deflect or absorb conventional kinetic and chemical munitions. Overcoming such shields would require high-energy, precision-directed solutions, highlighting the extreme physical robustness of these hypothetical systems (Cooper 1996).
6. **Multimodal Measurement Platform:** The development of a synchronized, multimodal sensing system combining magnetometry, spectroscopy, radiofrequency analysis, and physiological monitoring provides a replicable methodology for empirical UAP research. Integration of machine learning enhances the detection of rare and transient events while minimizing false positives. This approach lays the groundwork for future observational networks, enabling systematic data collection and hypothesis testing in a scientific framework (Peratt 1992; Teodorani 2024; Watters *et al.* 2023).
7. **Ground Interaction Signatures:** While primarily focused on airborne phenomena, the study acknowledges that near-ground or landing events may produce secondary diagnostic effects, such as localized thermal anomalies, minor magnetic remanence, subtle chemical modifications, and transient biological impacts. These signatures, though not central to the primary plasma-magnetic analysis, provide complementary avenues for empirical verification when accessible (Çalışkanoğlu *et al.* 2023; Genareau *et al.* 2019).

In conclusion, this study bridges theoretical modeling, observational diagnostics, and experimental methodology to provide a scientifically grounded platform for studying UAPs. While many proposed mechanisms involve extreme or speculative technologies, the convergence of plasma physics, high magnetic fields, and advanced materials science offers physically consistent explanations for the documented behaviors of UAPs. Further empirical research, guided by the multimodal platform described herein, will be crucial for validating these hypotheses and advancing UAP science from anecdotal reporting to rigorous, reproducible study.

At the present time, largely due to historical funding limitations for this line of research, the level of data precision and methodological sophistication now required—and emphasized in this work—has yet to be achieved. However, new, highly detailed projects (Teodorani 2024) as well as systematic monitoring campaigns are currently underway (Watters *et al.* 2023), and only the future (hopefully soon) will be able to provide answers at both the qualitative and quantitative levels of the physics we expect to obtain.

The ultimate goal of this research is not to prove or disprove that "technologies more advanced than human ones" are traversing our skies, but rather to learn something new to add to the great book of physics (and its technological applications), without necessarily invoking the existence of any "esoteric physics".

References

Adler, S. L. 1971. "Photon Splitting and Photon Dispersion in a Strong Magnetic Field." *Annals of Physics* 67 (2): 599–647.

Alfieri, F., *et al*. (2020). "Improving the detection sensitivity for Laser Induced Breakdown Spectroscopy (LIBS)". *Frontiers in Physics*.

Baines, K. H., *et al*. 2021. "Physical Characteristics of Possible Plasma-Based Propulsion". *Aerospace Science and Technology* 110: 106491.

Bekefi, G., and A. Barrett. 1977. Electromagnetic Vibrations, Waves, and Radiation. MIT Press. Chapters 13, 14 and 15.

Bellan, P. M. 2006. *Fundamentals of Plasma Physics*. Cambridge University Press. Chapters 11, 12 and 18.

Benford, J.; Swegle, J. A. and Schamiloglu, E. 2007. *High Power Microwaves*. CRC Press. Chapters 1, 7 and 10.

Benedetto, J. J. 1975. *Spectral Synthesis*. Academic Pr. Chapters 3 and 4.

Bornatici, M., *et al*. 1983. "Electron Cyclotron Emission and Absorption in Fusion Plasmas". *Nuclear Fusion* 23 (9): 1153.

Budker, D., *et al*. 2002. "Resonant Nonlinear Magneto-Optical Effects in Atoms". *Reviews of Modern Physics* 74 (4): 1153.

Çalışkanoğlu, A. Z., Camara, A. S. B., Cimarelli, C., Dingwell, D. B., & Hess, K.-U. 2023. "*Experimental generation of fulgurite under realistic lightning discharge conditions". Scientific Reports*, **13,** 11685.

Chen, F. F. 2016. *Introduction to Plasma Physics and Controlled Fusion*. Springer. Chapters 3, 7 and 8.

Choueiri, E. Y. 2009. "The Efficient Future of Deep-Space Travel-Electric Rockets". *Scientific American*, February 2009 Issue: https://www.scientificamerican.com/article/the-efficient-future-of-deep-space/

Cooper, P. W. 1996. *Explosives Engineering*. Wiley-VCH. Chapter 1.

Coumbe, Daniel. 2023. *Anomaly – A Scientific Exploration of the UFO Phenomenon*. Rowman & Littlefield.

Del Zanna, G., and H. E. Mason. 2018. "Solar UV and X-ray Spectral Diagnostics". arXiv:1809.01618.

Dove, N. C., Klingeman, D. M., Carrell, A. A., Cregger, M. A., & Schadt, C. W. 2021. "*Fire alters plant microbiome assembly patterns: integrating the plant and soil microbial response to disturbance". New Phytologis*t, 230, 2433–2446.

Ducharme, A. 2019. *IEEE Transactions on Plasma Science*.

Enoto, T., Wada, Y., Furuta, Y., Nakazawa, K., Yuasa, T., Okuda, K., Makishima, K., Sato, M., Sato, Y., Nakano, T., Umemoto, D., & Tsuchiya, H. 2017. "*Photonuclear reactions triggered by lightning discharge". Nature*, 551 (7681), 481–484.

Fedosin, S. G. and Kim, A. S. 2001. "The Physical Theory of Ball Lightning". *Applied Physics* (Russian Journal), No. 1: 69-87. https://www.researchgate.net/publication/236134349_The_ physical_theory_of_ball_lightning#fullTextFileContent

Genareau, K., Wardman, J., Wilson, T. M., McNutt, S. R., Izbekov, P., & co-authors. 2019. "*Effects of lightning on the magnetic properties of volcanic ash". Scientific Report*s, 9, 4726 (article number).

Ginzburg, V. L., and A. A. Rukhadze. 1972. *Waves in Magnetoplasma*. Pergamon Press.

Giri, D.V. and Tesche, F.M. 2004. "Classification of Intentional Electromagnetic Environments". *IEEE Transactions on Electromagnetic Compatibility*, 46, 322-328.

Glover, P. M., *et al*. 2007. "Vestibular Effects of Magnetic Field Exposure: A Working Model." *Bioelectromagnetics* 28 (5): 400–408.

Goksel, B., and M. Mashek. 2016. "First Breakthrough for Future Air-Breathing Magneto-Plasma Propulsion Systems". *Journal of Physics Conference Series*, 825 (1). DOI: 10.1088/1742-6596/825/1/012005

Gray, D. F. 2005. *The Observation and Analysis of Stellar Photospheres*. Cambridge University Press. Chapters 11, 12 and 16.

Greenewald, J. 2025. "The 1976 Iran Incident — primary sources and FOIA documents." *The Black Vault*. URL: https://www.theblackvault.com/casefiles/the-1976-iran-incident/#citations-and-sources

Griem, Hans R. 1974. *Spectral Line Broadening by Plasmas*. Academic Press Inc. Chapters 2, 6 and 8.

Haines, R. F. 2000. "Aviation Safety in America: A Previously Neglected Factor". *NARCAP TR 01-2000*, URL: https://static1.squarespace.com/static/5cf80ff422b5a90001351e31/t/5d02ea1772637c00014776c5/1560472092579/narcap.TR1.AvSafety.pdf

Harris, B., Dedrick, J. P., Niemi, K., & Wagenaars, E. 2024. "*Ozone production by an He+O_2 radio-frequency atmospheric-pressure plasma jet driven by tailored voltage waveforms". Plasma Sources Science and Technology*, 33, 075020.

Hendry, A. 1979. *The UFO Handbook: A Guide to Investigating, Evaluating and Reporting UFO Sightings.* Doubleday.

Herlach, F., and N. Miura. 2003. *High Magnetic Fields: Science and Technology*. World Scientific. Chapters 1, 8 and 10.

Hershcovitch, A. 1995. "Plasma Window as a Vacuum–Atmosphere Interface". *Physics of Plasmas* 2: 2135.

International Commission on Non-Ionizing Radiation Protection (ICNIRP), 2013. *Guidelines on Limits of Exposure to Incoherent Visible and Infrared Radiation.* Health Physics, 105(1): 74–96, 2013. DOI: 10.1097/HP.0b013e318289a611

ICNIRP (International Commission on Non-Ionizing Radiation Protection). 2013. "Guidelines on Limits of Exposure to Incoherent Visible and Infrared Radiation." *Health Physics* 105(1): 74–96. DOI: 10.1097/HP.0b013e318289a611.

ICNIRP (International Commission on Non-Ionizing Radiation Protection). 2020. "Guidelines for Limiting Exposure to Electromagnetic Fields (100 kHz to 300 GHz)". *Health Physics* 118(5): 483–524. DOI: 10.1097/HP.0000000000001210.

Jackson, J. D. 1998. *Classical Electrodynamics*. 3rd ed. Wiley. Chapters 7, 9, 12 and 14.

Jefferies, J. T., and D. L. Mickey. 1991. "The Observation and Analysis of Zeeman Splitting in Solar Lines". *Astrophysical Journal* 372: 694–701.

Kaiser, K. L. 2004. *Electromagnetic Compatibility Handbook*. CRC Press. Chapters 1, 13 and 17.

Knuth, Kevin H.; Powell, Robert M. & Reali, Peter A. 2019. "Estimating Flight Characteristics of Anomalous Unidentified Aerial Vehicles". *Entropy* 21, no. 10: 939.

Knuth, K: H.; Ailleris, P.; Agrama, H. A.; Ansbro, E.; Budinger, P. A.; Cai, T.; Canuti, T.; Cifone, M. C.; Cornet, W. B.; Courtade, F. *et al*. 2025. "The new science of Unidentified Aerospace-Undersea Phenomena (UAP)". *Progress in Aerospace Science* 156, 101097. https://www.sciencedirect.com/science/article/abs/pii/S0376042125000235

Kruer, W. L. 1988. *The Physics of Laser-Plasma Interactions*. Westview Press. Chapters 4 and 5.

Landi Degl'Innocenti, E., and Landolfi, M. 2004. *Polarization in Spectral Lines*. Springer, Astrophysics and Space Science Library, Vol. 307.

Lang, K. R. 1991. *Astrophysical Formulae: A Compendium for the Physicist and Astrophysicist.* Springer Verlag. Vol. 1: Chapters 2 and 5; Vol. 2: Chapter 12.

Lieberman, M. A., and A. J. Lichtenberg. 2005. *Principles of Plasma*

Discharges. Wiley. Chapters 3 and 10.

Maccabee, Bruce S. 1994. "Strong magnetic field detected following a sighting of an unidentified flying object". *Journal of Scientific Exploration*, 8, no. 3: 347-65.

Maccabee, Bruce S. 1999. "Optical power output of an unidentified high altitude light source". *Journal of Scientific Exploration* 13, no. 2: 199-211.

Masters, R. A. 2014. "High resolution slit-free direct-viewing multiplexing field spectrograph". US Patent US8749781B2. https://patents.google.com/patent/US20120287430.

Meessen, A. 2011. "*The Belgian Wave and the photos of Ramillies*". PDF file downloadable after clicking on this exact title on Google search (source: "Das UFO-Phänomen").

Meessen, Auguste. 2012a. "Pulsed EM Propulsion of Unconventional Flying Objects". In *PIERS 2012 Proceedings* Moscow, Russia, August 19–23, 2012.

Meessen, Auguste. 2012b. "Evidence of Very Strong Low Frequency Magnetic Fields". In *PIERS 2012 Proceedings* Moscow, Russia, August 19–23, 2012: 524-28. http://www.cobeps.org/pdf/meessen_evidence.pdf

NASA NTRS (Technical Reports Server). "MPD Propulsion Research". URL: https://ntrs.nasa.gov/citations/19910022848

NASA. 2023. "UAP Independent Study Team Report". URL: https://science.nasa.gov/wp-content/uploads/2023/09/uap-independent-study-team-final-report.pdf

NASEM (National Academies of Sciences, Engineering, and Medicine). 2007. *Plasma Science: Advancing Knowledge in the National Interest.* Washington, DC: The National Academies Press.

National Radiological Protection Board (UK). 2004. "Advice on Limiting Exposure to EM Fields".

Neukart, F. 2023. "Magnetic Fusion Plasma Drive. arXiv: 2309.11524v3ka

NICAP. 1964. *The UFO Evidence: A Thirty-Year Report*. URL: https://www.nicap.org/ufoe/UFO%20Evidence%201964.pdf

Nolan, G. P.; Vallee, J. F.; Jiang, S. & Lemke, L. G. 2022. "Improved instrumental techniques, including isotopic analysis, applicable to the characterization of unusual materials with potential relevance to aerospace forensics". *Progress in Aerospace Science* 128 (2022) 100788.

ODNI (Office of the Director of National Intelligence). 2021. "Preliminary Assessment: Unidentified Aerial Phenomena". URL: https://www.dni.gov/files/ODNI/documents/assessments/Prelimary-Assessment-UAP-20210625.pdf

Pasek, M. A., & Block, K. (2009). "*Lightning-induced reduction of phosphorus oxidation state*". *Nature Geoscience*, 2(8), 553–556.

Peratt, A. 1992. *Physics of the Plasma Universe*. Springer. Chapters 3, 5 and 8.

Persinger, M. A. 2001. "The Neuropsychiatry of Paranormal Experiences." Journal of Neuropsychiatry and Clinical Neurosciences 13 (4): 515–524.

Persinger, M. A. (2002). "Experimental Simulation of the God Experience". In *NeuroTheology: Brain, Science, Spirituality, Religious Experience* (edited by Rhawn Joseph – California University Press): http://www.neurosciarchive.byethost12.com/2003-Persinger-Neurotheology-Brain-Science-Spirituality-Religious-Experience-Experimental-simulation-of-the-God-experience.pdf?i=1

Privat-Maldonado, A., Schmidt, A., Lin, A., Weltmann, K.-D., Wende, K., Bogaerts, A., & Bekeschus, S. (2019). "*ROS from physical plasmas: redox chemistry for biomedical therapy*". *Oxidative Medicine and Cellular Longevity*, 2019, 9062098.

Project Condign Report. 2000. UK Ministry of Defence.

Reilly, J. P. 1998. *Applied Bioelectricity: From Electrical Stimulation to Electropathology*. Springer. Chapters 2 and 11.

Rodeghier, Mark. 1981. *UFO reports involving vehicle interference : a catalogue and data analysis.* Center for UFO Studies (CUFOS).

Rutledge, H. D. 1982. *Project Identification: The First Scientific Field Study of Ufo Phenomena.* Prentice Hall Direct.

Rüedi, I.; Solanki, S. K. and Livingston, W. 1995. "Infrared Lines as Probes of Solar Magnetic Features". *Astronomy and Astrophysics* 293: 252–262.

Schenck, J. F. 2000. "Safety of strong, static magnetic fields"**.** *Journal of Magnetic Resonance Imaging*, 12(1), 2–19.

Seol, Y.-B., Kim, J., Park, S.-H., & Chang, H.-Y. 2017. "*Atmospheric-pressure pulsed plasma induces cell death in photosynthetic organs via intracellularly generated ROS*". *Scientific Reports*, 7, 589.

Sharma, V. P., Kesari, K. K., & Behari, J. 2010. "*Effects of mobile phone radiation on reproductive biology of male rats and oxidative stress in plants". Electromagnetic Biology and Medicine*, 29(1), 26–30. https://doi.org/10.3109/15368370903507979

Shellock, F. G. 2002. "Magnetic Resonance Procedures and Biomedical Implants: Safety Considerations". *Seminars in Musculoskeletal Radiology* 6 (3): 257.

Schütze, A., Jeong, J. Y., Babayan, S. E., Park, J., Selwyn, G. S., & Hicks, R. F. 1998. "*The atmospheric-pressure plasma jet: A review and comparison to other atmospheric-pressure plasma sources". IEEE Transactions on Plasma Science***, *26***(6), 1685–1694.

Stenhoff, Mark. 1999. *Ball Lightning: An Unsolved Problem in Atmospheric Physics.* Springer. Chapters 6 and 9.

Stix, T. H. 1992. *Waves in Plasmas*. Springer. Chapters 7 and 10.

Stenflo, J. O. 1994. *Solar Magnetic Fields: Polarized Radiation Diagnostics*. Springer, Astrophysics and Space Science Library, Vol. 189.

Strand, E. P. 1984. "Project Hessdalen" 1984 – Final Technical Report". *Project Hessdalen* website. https://old.hessdalen.org/reports/hpreport84.shtml

Tajmar, M. 2002. *Advanced Space Propulsion Systems and Technologies*. Springer Aerospace Briefs. Chapters 5 and 8.

Tedesco, J. & Tedesco G. 2024. "Unraveling Mystique: LongDelay Echoes; Anomalous Propagation of Radar Signals under the Influence of Unidentified Anomalous Phenomena". *Open Journal of Applied Sciences*, Vol. 14(12), pp. 3618–3648. URL: https://www.scirp.org/journal/paperinformation?paperid=138426

Teodorani, M. 2000. "Physical data acquisition and analysis of possible flying extraterrestrial probes by using opto-electronic devices". *Extraterrestrial Phys.* Rev. 1, no. 3: 32-37.

Teodorani, M. 2004. "A long-term scientific survey of the Hessdalen phenomenon". *Journal of Scientific Exploration*, 18, no. 2: 217-51.

Teodorani, M. 2024. "Investigating UAP Events Using Astronomical Techniques". *Limina – The Journal of UAP Studies* 1(1), 40-54.

Teodorani, M. 2025. "On the Hypothesis of Interactive Plasma Phenomena". Workshop: *Process Philosophy, Plasma Cosmology, and Transpersonal Psychology*, July 24-27, 2025, Exeter Univ., UK. In press.

Tkachenko, Y., *et al*. 2023. "MHD Simulations of Magnetoplasmadynamic Thruster". Conference: 59th Culham Plasma Physics Summer School.

Tomko, J. A., Johnson, M. J., Boris, D. R., Petrova, T. B., Walton, S. G., & Hopkins, P. E. 2022. "*Plasma-induced surface cooling". Nature Communications*, 13, 2623.

Tsakadze, J. S. 1999. *Physics of High-Density Z-Pinch Plasmas*. Springer. Chapters 3 and 8.

Vallée, Jacques. 1998. "Estimates of Optical Power Output in Six Cases of Unexplained Aerial Objects with Defined Luminosity Characteristics". *Journal of Scientific Exploration* 12(3): 345-358.

Vallée, Jacques. F.; Dini, Luc, and Mestchersky, Geoffrey. 2025. "Estimates of radiative energy values in ground-level observations of an unidentified aerial phenomenon: New physical data". *Progress in Aerospace Science* 156, 101098

Wada, Y., Enoto, T., Nakazawa, K., Odaka, H., Furuta, Y., Tsuchiya, H., & co-authors. 2020. "*Photonuclear reactions in lightning: 1. Verification and modeling of reaction and propagation processes". Journal of Geophysical Research: Atmospheres*, 125, e2020JD033193.

Walters, P. W. & Zukas J. A. 1989. *Fundamentals of Shaped Charges*. Wiley-

Interscience. Chapters 4 and 9.
Watters, W. A.; Loeb, A.; Laukien, F.; Cloete, R.; Delacroix, A.; Dobroshinsly, S.; Horvath, B.; Kelderman, E.; Little, S.; Masson, E., *et al.* 2023. "The Scientific Investigation of Unidentified Aerial Phenomena (UAP)". *Journal of Astronomical Instrumentation* 12, no. 1, 2023, 2340006: https://www.worldscientific.com/doi/epdf/10.1142/S2251171723400068
WHO (World Health Organization). 2006. "Electromagnetic Fields and Public Health: Static Fields". https://www.who.int/peh-emf/publications/facts/fs299/en/.
Wiley, A., *et al.* 2007. "Remote Sensing of the Spatial and Temporal Structure of Magnetic Reconnection in the Magnetosphere". *Reviews of Geophysics*.
Zeeman, P. 1897. "The Effect of Magnetisation on the Nature of Light Emitted by a Substance." *Philosophical Magazine* 43 (262): 226–239.
Zhang, T., *et al.* 2021. "UAV Inlet Plasma Stealth Numerical Simulation". *Journal of Physics Conf. Series*, 1786 (2021) 012040. DOI:10.1088/1742-6596/1786/1/012040

APPENDIX A – Simulated Scenarios: Quantitative, Instrument-Testable Cases

This appendix presents three short reference scenarios illustrating how multi-instrument observations (high-resolution spectroscopy, photometry, radar, RF analysis, magnetometry, particle detection) respond to different classes of transient aerial phenomena. Each scenario begins with the *explicit equations* used in the analysis, followed by a concise numerical discussion. Each case ends with a falsifiable hypothesis, parameter bounds, and null-test provisions.

- **Scenario 1 — Slowly Moving 1-m Object at 1 km, 100 kW Optical Output, 30 s Duration**

A small (1-m) object, radiating 100 kW, moves slowly with slight wobbling for 30 s at close range (1 km). It can be easily tracked by a Pan Tilt Zoom camera connected to a spectrograph via fiber optics. Its luminosity is stable enough for high-resolution spectroscopy, and the received flux is easily sufficient to reach S/N ≳ 10 in very short exposures. Zeeman splitting is measurable if even modest magnetic fields are present, and simultaneous sensors (magnetometers, RF, cameras) can be synchronized to the spectral variability on sub-second timescales. This scenario is ideal for obtaining high-quality, diagnostic spectroscopy, allowing robust magnetic-field measurements and straightforward falsification of any magnetoplasma model if Zeeman signatures or correlated EM effects are absent.

The following main equations are used:

$$b = \frac{L}{4\pi d^2}$$ Irradiance

$$P_{\text{coll}} = b\, f_{\text{vis}}\, A$$ Collected Visible Power

$$\dot{N} = \frac{P_{\text{coll}}}{hc/\lambda}$$ Photon Rate at Wavelength

$$\Delta\lambda_{\text{res}} = \frac{\lambda}{R}$$ Instrumental Spectral Resolution

$$\Delta\lambda_Z = \frac{e\lambda^2 g B}{4\pi m_e c}$$ Zeeman Splitting

$$\delta\lambda_{\text{centroid}} \approx \frac{\Delta\lambda_D}{2.35\,\text{SNR}}$$ Centroid Precision

These are the main variables:

L = luminosity

d = distance

A = camera lens area = 0.20 m²

f_{VIS} = visible fraction = 0.1

$R = \lambda/\Delta\lambda$ = spectral resolving power = 5×10^4

$\lambda/\Delta\lambda_D$ = thermal Doppler width

B = magnetic field, g = Landé factor (2.5 for Fe I 15648 Å)

In such a situation, the irradiance is b = 10^{-3} Wm^{-2}. With f_{VIS} = 0.1, the camera receives P_{coll} = 1.6 x 10^{-4} W, corresponding to N ≈ 5 x 10^{14} s^{-1} photons across the visible band and ~ 10^9 s^{-1} per spectral resolution element after throughput. Even weak emission lines carrying ~ 1% of the visible flux reach SNR = 10 in ~ 1-5 ms.

For Fe I 15648 Å, a 1-T magnetic field produces $\Delta\lambda_Z$ ≈ 2.86 Å, far exceeding the thermal width $\Delta\lambda_D$ ~ 0.05-0.15 Å. Centroid precision at SNR = 10 is $\delta\lambda_{CENTROID}$ ~ (4-7) X 10^{-3} Å, equivalent to velocity precision 200-300 m s^{-1} and a magnetic field sensitivity of a few milliTesla.

Radar and RF instruments in this low-luminosity case would detect little unless the plasma sheath becomes denser than n_e ~ 10^9 – 10^{10} cm^{-3}, which is unlikely at 100 kW. Magnetometers might detect extremely weak coupling;

particle detectors likely register no flux.

As falsifiable hypotheses and bounds, we can say this: 1) If the UAP possesses a coherent magnetic sheath of B ≥ 0.1 T, then Fe I 15648 Å must show detectable Zeeman separation ≥ 0.3 Å under these observing conditions; 2) If plasma density exceeds $n_e \sim 10^{10}$ cm^{-3}, then radar reflection or attenuation at GHz frequencies must occur.

As null-test calibration, repeat observations on Venus, bright stars, aircraft strobes, and ionospheric reflections are carried out to verify absence of spurious Zeeman signatures or RF/magnetic coincidences. As a falsification criterion, if no Zeeman splitting, no RF/magnetic activity, and no thermal excess are detected, then strong magnetic/plasma-dominated propulsion at 100 kW is ruled out.

- ***Scenario 2 — Fast Object at 10 km, 50 MW Brightness, B Oscillating 1–100 T, 60 s Duration***

A bright (50 MW) fast-moving object shows a magnetic field oscillating between 1 and 100 T for about 60 s, observed (for better object tracking accuracy) with a slitless spectrograph (R=10,000) and with throughput h = 0.1, connected to a tracking PTZ camera via fiber optics. The high luminosity and stable tracking allow the acquisition of hundreds to over one thousand time-resolved spectra, each with S/N ≥ 10. Large Zeeman variations appear over time and can be directly cross-checked with magnetometer and RF fluctuations. This scenario provides strong time-domain constraints: correlated oscillations in spectral Zeeman splitting, magnetic sensors, and RF output would strongly support a magnetically driven plasma mechanism; their absence would decisively reject it.

Key equations used are same as Scenario 1, with slightly lower resolving power ($R = 10^4$). What comes out is as follows. The irradiance is b = 4.0 x 10^{-2} Wm^{-2} and the system receives ~ 10^{15} photons per second in the visible band. With $R = 10^4$, exposures of 50-100 ms easily achieve SNR = 10 per resolution element while maintaining reliable tracking. Thus, a 60-s event yields: $N_{SPEC} \approx 600 - 1200$ spectra. For Fe I 15648 Å: $\Delta\lambda_Z(1T)$ » 2.86 Å and $\Delta\lambda_Z(100T) \approx 286$ Å, which are fully resolved at $\Delta\lambda_Z$ » 1.56 Å.

The changing Zeeman pattern $\Delta\lambda_Z(t)$ traces the magnetic oscillation directly. Magnetometers may detect synchronous low-frequency field excursions. RF analyzers may register plasma-driven broadband emission or harmonics, especially during the 100-T peaks. Radar detectability depends on plasma density. GHz cutoff requires $n_e \geq 10^{10}$ cm^{-3}.

As falsifiable hypotheses and bounds, we can say this: 1) If the UAP's magnetic field truly oscillates between 1–100 T, then the observed Zeeman splitting must vary between 2.86 Å and 286 Å with a measurable temporal pattern matching *B(t)* as measured in distance by the magnetometer; 2) If plasma densities rise above 10^{10} cm^{-3}, then the radar system must show corresponding attenuation/echo modulation.

As null tests calibrations, it is necessary to track satellites, bright stars, aircraft, lightning, and meteor trails with the same PTZ-slitless system (camera plus spectrograph), verifying that no spurious Zeeman splitting, RF bursts, or magnetic excursions appear. As a falsification criterion, a constant or absent Zeeman signature, uncorrelated RF activity, and no magnetometer response definitively exclude 1–100 T coherent fields in a 50-MW system.

- ***Scenario 3 — Slow 10-m Object at 2 km, 1-kW Steady State; 5-s Burst to 10 MW and 10 T***

A large (10-m) weakly luminous object (1 kW) moves slowly for 3 minutes with a steady 1-T magnetic field. It then undergoes a 5-s outburst to 10 MW luminosity, 10-T magnetic field, and greatly increased plasma density. Slitless spectrograph with R = 5 x 10^4 is connected to PTZ camera via fiber optics. Spectral line visibility improves by four orders of magnitude during the burst, Zeeman splitting increases sharply, and radar, RF, and magnetometer signals show corresponding abrupt changes. The multi-instrument response cleanly separates pre-burst and burst regimes. The sudden, synchronized jump in luminosity, Zeeman splitting, radar reflectivity and magnetic signatures provides a clear, multi-modal test for magnetic–plasma outbursts: with this instrumentation, such an event would be unmistakable if real, and its absence would rule out the underlying physical interpretation.

Key equations used are same as Scenarios 1 and 2, but with the addition of the plasma cutoff relation given by:

$f_p \approx 8980\sqrt{n_e\ (\mathrm{cm}^{-3})}$, which determines radar reflectivity

What comes out is as follows. At d = 2 km, b_{init} = 2 x 10^{-5} Wm^{-2}, $t_{SNR=10,\ init}$ ~ 2 ms for a typical line. Suddenly, luminosity rises to L = 10 MW and the magnetic field jumps to B = 10 T for 5 s, so that b_{burst} = 2 x 10^{-1} Wm^{-2} and $t_{SNR=10,\ burst}$ ~ 10^{-7} ms (photon-noise limit; practical exposures are ~ 0.1-1 ms).

Zeeman splitting is: $\Delta\lambda_Z$ (1 T) = 2.86 Å and $\Delta\lambda_Z$ (10 T) = 28.6 Å, well above thermal $\Delta\lambda_D \sim 0.05 - 0.15$ Å. Plasma-density increase may raise f_p into the GHz range, producing radar blackout or strong reflection. Microwave spectra may show transient broadband spikes or harmonic structures. Magnetometers may detect short magnetic pulses; particle detectors may register increased flux if the sheath produces energetic ions or electrons.

As falsifiable hypotheses and bounds, we can say this: 1) If the burst field reaches 10 T, then Zeeman splitting must increase by a factor 10 between pre-burst and burst phases (2.86 Å —> 28.6 Å); 2) If the plasma density becomes high enough for GHz cutoff, then radar must show measurable attenuation or reflection changes during the 5-s burst.

As null tests calibrations, it is necessary to verify against aircraft, satellites, and lightning discharges that no such multi-channel correlation (spectral–magnetic–RF–particle) occurs in normal atmospheric transients. As a falsification criterion, absence of step-change Zeeman splitting and radar/RF modifications during the 5-s luminous burst rules out the hypothesized jump to 10 T and the associated plasma-density increase.

Each scenario above is expressed as a set of falsifiable hypotheses with specific numerical thresholds tied to instrument performance:

- Zeeman constraints provide direct, linearly interpretable bounds on magnetic-field strength at the milliTesla level.
- Photon budgets and SNR calculations determine minimum exposure times, ensuring that detection claims are grounded in achievable data quality.
- Radar and RF behavior impose independent, wavelength-specific constraints on plasma frequency and therefore n_e.
- Magnetometer and particle-detector correlations provide third-party verification of EM or plasma dynamics.

Corresponding null tests (bright planets, satellites, aircraft, meteor trails, controlled ionospheric reflections) establish expected background behavior and ensure that any detected correlation between spectra, magnetic fields, RF activity, and particle counts is non-instrumental and therefore physically meaningful.

Together, these scenarios demonstrate precisely what must be demanded by a rigorous scientific research: numerically bounded, calculable, falsifiable observational predictions grounded in standard plasma physics, radiative transfer, and instrumental sensitivity.

APPENDIX B – Null-experiment & Calibration Protocol

To ensure that any detected anomaly is genuinely physical and not an artefact of instrumentation, all observations must be anchored to a rigorous calibration and null-testing protocol. The following procedures are required for each observing session to guarantee the reliability, traceability, and reproducibility of the acquired data:

1. **Wavelength calibration**

Conduct Th–Ar or He–Ar arc-lamp exposures immediately before and after each observing block to secure a stable dispersion solution. Where available, use a laser frequency comb (LFC) to obtain SI-traceable wavelength calibration with sub-m s^{-1} repeatability. This ensures that Zeeman splitting, Doppler shifts, and line-profile evolution can be measured without systematic drifts.

2. **Instrumental profile characterization**

Acquire narrow, unresolved lamp lines (or LFC modes) to determine the nightly instrumental profile (IP). The IP must be recorded and used in subsequent deconvolution to extract intrinsic spectral-line shapes, widths, and polarimetric signatures. This is essential for measuring small Zeeman or Stark components.

3. **Radiometric and flat-field calibration**

Observe standard spectrophotometric stars for absolute flux calibration, and employ high-S/N lamp flats to correct for pixel-to-pixel sensitivity and wavelength-dependent throughput. This ensures that variations in brightness or continuum slope are physically meaningful, not instrumental.

4. **Magnetometer calibration**

Calibrate all magnetometers using a site-level Helmholtz coil, recording current–field conversion curves and the full 3-axis response. Perform both DC and AC (search-coil) checks. This enables quantitative comparison between magnetic-field variations inferred from Zeeman spectroscopy and those measured directly in situ.

5. **Radio-frequency (RF) system calibration**

Use a calibrated thermal noise source and antenna gain chart to determine the system temperature and verify absolute sensitivity. This allows conversion from received power to brightness temperature, crucial for distinguishing electromagnetic transients from noise spikes or RFI.

6. **Radar calibration**

Perform radar cross-section (RCS) checks using a corner reflector and predefined targets to calibrate gain, dynamic range, and polarimetric response. This provides a baseline for interpreting potential UAP radar signatures such as plasma cutoff, absorption, or anomalous reflectivity.

7. **Null experiments**

A series of controlled non-anomalous tests is required to quantify false positives and validate the end-to-end instrument chain:

- **(a)** Observe bright planets (Venus, Jupiter) and predictable satellite reflections (*e.g.*, remaining Iridium flares) to confirm proper photometric, spectral, and timing behavior.
- **(b)** Track aircraft with known ADS-B data to test motion-classification algorithms and verify trajectory reconstruction accuracy.
- **(c)** Schedule control runs during known ionospheric disturbances (solar flares, geomagnetic storms) to characterize the system's response to natural plasma variations.
- **(d)** Conduct "blank-sky" observations with no intentional sources to measure the background false-alarm rate for optical, RF, radar, and magnetic sensors.

8. **Pre-registration of hypotheses**

Prior to data acquisition, define a limited set of explicit, falsifiable criteria—for example, detectability of Zeeman splitting greater than 0.3 Å in Fe I 15648 Å at S/N ≥ 10, or RF bursts exceeding 5*s* above baseline. Pre-registration minimizes post-hoc bias and ensures that any claimed detection passes objective, pre-defined thresholds. Here are some examples:

- If $B \geq 0.1$ T near the emitting sheath, then Fe I 15648 Å will show $\Delta\lambda_Z \geq 0.286$ Å; detection requires $R \geq 50{,}000$ and per-element $S/N \geq 10$.
- If broadband synchrotron emission produces $L_{vis} \geq 10$ MW at $d \leq 10$ km, a 10-cm optical system (10 s exposure, $\eta = 0.1$) will achieve $S/N \geq 10$ for continuum spectroscopy.
- If $n_e \geq 10^{11}$ cm^{-3} locally, radar returns at S-band (2–4 GHz) will show reflection/attenuation consistent with plasma cutoff and RCS increase $>3\sigma$ relative to baseline.
- Null hypothesis: pointing at bright planet targets (Venus, Jupiter) produces no correlated magnetometer transients above 3 nT baseline; any claimed UAP magnetometric signal must exceed this null distribution.